

1 **Determining Key Model Parameters of Rapidly Intensifying**
2 **Hurricane Guillermo(1997) using the Ensemble Kalman Filter**

3 HUBERTO C. GODINEZ* AND JON M. REISNER

Los Alamos National Laboratory, Los Alamos, New Mexico

4 ALEXANDRE O. FIERRO

Earth and Environmental Sciences division/Space and Remote Sensing Group, Los Alamos National Laboratory, Los Alamos, New Mexico

NOAA/Cooperative Institute for Mesoscale Meteorological Studies, Norman, Oklahoma

5 STEPHEN R. GUIMOND

Center for Ocean-Atmospheric Prediction Studies, Florida State University, Tallahassee, Florida

6 JIM KAO

Los Alamos National Laboratory, Los Alamos, New Mexico

* *Corresponding author address:* Humberto C. Godinez, Los Alamos National Laboratory, MS B284, Los Alamos, NM 87545.

E-mail: hgodinez@lanl.gov

ABSTRACT

7
8 In this work we determine key model parameters for rapidly intensifying Hurricane Guillermo
9 (1997) using the Ensemble Kalman Filter (EnKF). The approach is to utilize the EnKF as
10 a tool to only estimate the parameter values of the model for a particular data set. The
11 assimilation is performed using dual-Doppler radar observations obtained during the period
12 of rapid intensification of Hurricane Guillermo. A unique aspect of Guillermo was that during
13 the period of radar observations strong convective bursts, attributable to wind shear, formed
14 primarily within the eastern semicircle of the eyewall. To reproduce this observed structure
15 within a hurricane model, background wind shear of some magnitude must be specified; as
16 well as turbulence and surface parameters appropriately specified so that the impact of the
17 shear on the simulated hurricane vortex can be realized. To identify the complex nonlinear
18 interactions induced by changes in these parameters, an ensemble of model simulations have
19 been conducted in which individual members were formulated by sampling the parameters
20 within a certain range via a Latin hypercube approach. The ensemble and the data, derived
21 latent heat and horizontal winds from the dual-Doppler radar observations, are utilized in the
22 EnKF to obtain varying estimates of the model parameters. The parameters are estimated
23 at each time instance, and a final parameter value is obtained by computing the average
24 over time. Individual simulations were conducted using the estimates, with the simulation
25 using latent heat parameter estimates producing the lowest overall model forecast error.

26 **1. Introduction**

27 Hurricanes are among the most destructive and costliest natural forces on Earth and
28 hence it is important to improve the ability of numerical models to forecast changes in
29 their track, intensity, and structure. But, accurate prediction depends on minimizing errors
30 associated with initial, environmental, and boundary conditions, numerical formulations,
31 and physical parameterizations. Though significant progress has been made over the past

32 decade with regard to using data assimilation to primarily improve the initial state of a
33 hurricane (Zhang et al. (2009); Torn and Hakim (2009); Zou et al. (2010)), uncertainties still
34 remain in other aspects of hurricane prediction.

35 One source of uncertainty within hurricane models come from parameters, which domi-
36 nate the long-term behavior of the model. To explore whether these long-term uncertainties
37 can be reduced, model parameters associated with both environmental and physical forc-
38 ings are estimated for sheared hurricane Guillermo (1997, see Fig. 1) through the use of the
39 ensemble Kalman filter (EnKF). Specifically, four parameters describing momentum sinks
40 and moisture sources in the planetary boundary-layer, the unresolved transport of these
41 quantities away from the boundary-layer, and a parameter associated with describing the
42 wind shear impacting Guillermo will be estimated. One of the key points of this paper is
43 to illustrate that parameter uncertainty contributes significantly to the overall long-term
44 uncertainty in a hurricane simulation.

45 Various authors (Anderson (2001); Annan et al. (2005); Hacker and Snyder (2005); Aksoy
46 et al. (2006b); Aksoy et al. (2006a); Tong and Xue (2008); Hu et al. (2010); Nielsen-Gammon
47 et al. (2010)) have documented the ability of the EnKF procedure to simultaneously evaluate
48 model state and parameters. In these papers, the parameters are included as part of the
49 model state in the assimilation. This combination of evolving elements (model variables) and
50 non-evolving elements (model parameters) within the analysis introduces some difficulties for
51 parameter estimation, such as parameter collapse and assimilation divergence. To mitigate
52 these difficulties, the parameters are inflated to a prespecified variance, so as to avoid the
53 collapse and keep a reasonable spread in the parameters. These techniques have proven to be
54 effective for parameter estimation, but they require adjustments and tuning of the inflation to
55 obtain good estimates. The approach in our current paper differs from previous work in the
56 sense that the parameters and model state are not combined in the assimilation procedure in
57 order to estimate the parameters. In this work we use the EnKF as a tool to only estimate
58 key model parameters for a given time-distributed observational data set. Furthermore, since

59 the parameters are assumed to be non-evolving, they are estimated independently from each
60 observational data set in time. Once the parameters are estimated at each time instance
61 where observations are available, a final estimate is obtained by computing the time average
62 value. A key aspect is to explore if estimating parameters through EnKF data assimilation
63 can improve model simulation, especially for such a highly non-linear problem as a hurricane.
64 To test the applicability and viability of this approach, a twin-experiment is performed for a
65 hurricane model, where results indicate that the correct parameter values are recovered when
66 considering sufficient observational data. It must be noted that the parameter estimates
67 presented in the current work depends on two important factors: the numerical model being
68 utilized, and the data set being assimilated. Nevertheless, this technique is applicable for
69 estimating model parameters for any model and data set, as long as the parameters have a
70 strong connection to the type of observational data being used to estimate them.

71 One of the best dual-Doppler radar data sets (Reasor et al. (2009); Sitkowski and Barnes
72 (2009)) obtained within a hurricane will be used to estimate the parameters through assim-
73 ilation. Some unique aspects of Guillermo’s dual-Doppler radar data were that data from
74 10 flight legs over a six hour time period were individually processed to address temporal
75 variability and both derived fields of horizontal winds and latent heating (Guimond et al.
76 (2011)) were constructed from the flight legs. Taken together this observational data will be
77 used to quantify temporal variability in the four parameter estimates along with how these
78 estimates change depending on which observational field is utilized. Note that assessing
79 the temporal variability of the four parameters is important with regard to addressing the
80 effectiveness of parameter estimation within this highly nonlinear system.

81 An important test of the viability of the particular approach and data used to estimate
82 the parameters, is their ability to improve the solution of a hurricane model. To investigate
83 this issue, three simulations were run using temporally averaged values of the parameters
84 obtained from either derived observational field, (horizontal winds or latent heat) or both
85 fields. Hence, the final point of this paper will be to illustrate whether or not the parameter

86 estimates improved overall model predictability with regard to the type of observations being
87 assimilated.

88 The paper is organized as follows; Section 2 first describes the predictive component of the
89 parameter estimation model including the analytic equation set of the hurricane model, the
90 four model parameters present within this predictive model, the discretization, and a brief
91 overview of the EnKF data assimilation method. In Section 3 we describes various aspects
92 of the parameter estimation model setup including the ensemble setup and the processing
93 of the derived observational data fields. Section 4 is broken up into three sub-sections with
94 each section showing results relating to the three major points of this paper. A summary
95 and final remarks are presented in Section 5.

96 **2. Parameter estimation model**

97 The parameter estimation model is comprised of a predictive model and an parameter
98 estimation model. The chosen predictive model is the Navier-Stokes equation set coupled
99 to a bulk cloud model with the four parameters utilized within this model, whereas the
100 parameter estimation model employs the EnKF data assimilation. In addition to describing
101 their representative analytical representations, discussions regarding their respective discrete
102 formulations will also be presented in this section.

103 *2.a. Predictive model*

104 2.A.1) NAVIER-STOKES EQUATION SET

105 Since the analytical equation set representing the momentum, energy, and mass of the
106 gas phase is identical to that utilized in Reisner and Jeffery (2009), RJ hereafter, interested
107 readers can examine this manuscript for details regarding its formulation. Likewise the
108 primary difference between the equation set found in that paper and the current equation

109 set are additional terms associated with buoyancy in the vertical equation of motion related
 110 to various hydrometers, i.e., $g(\rho' + \rho_c + \rho_r + \rho_i + \rho_s + \rho_g)$ where g is gravity, ρ' is a density
 111 perturbation, ρ_c is the cloud water density, ρ_r is the rain water density, ρ_i is the ice water
 112 density, ρ_s is the density of snow, and ρ_g is the graupel density, with the next section briefly
 113 describing the bulk microphysical model used to predict the evolution of the hydrometers.

114 2.A.2) BULK MICROPHYSICAL MODEL

115 The mass conservation equation for a given particle type, $\rho_{part} = \rho_c, \rho_r, \rho_i, \rho_s, \rho_g$, within
 116 the bulk microphysical model can be written as follows

$$\frac{\partial(\rho_{part})}{\partial t} + \frac{\partial[(u^{i'} - wfall_{part}\delta_{i'3})\rho_{part}]}{\partial x^{i'}} = fdensity_{part} + \frac{\partial F_{\rho_{part}}^{i'}}{\partial x^{i'}}, \quad (1)$$

117 where $u^{i'}$ are fluid velocities in each spatial direction and the last term represents the tur-
 118 bulent diffusion of a particle type using a diffusion coefficient diagnosed from a turbulence
 119 kinetic energy (TKE) equation, see Eq. 3 in Reisner and Jeffery (2009).

120 The conservation equation for either cloud droplet number (N_c) or ice particle number
 121 (N_i), $N_{part} = N_c, N_i$, can be written as follows

$$\frac{\partial(N_{part})}{\partial t} + \frac{\partial[(u^{i'} - wfall_{part}\delta_{i'3})N_{part}]}{\partial x^{i'}} = fnumber_{part} + \frac{\partial F_{N_{part}}^{i'}}{\partial x^{i'}}, \quad (2)$$

122 where $wfall_{part}$, $fdensity_{part}$, and $fnumber_{part}$ represent the fall speed, density, and number
 123 sources or sinks from the bulk microphysical model for a given particle type, a hybrid of the
 124 activation and condensation model found in Reisner and Jeffery (2009) together with all of
 125 the other relevant bulk parameterizations found in Thompson et al. (2008). Note, because
 126 of significant differences in the particle distributions between winter storms and hurricanes,
 127 the slope-intercept formulas were modified following McFarquhar and Black (2004).

129 The initialization of the environmental or background horizontal homogeneous potential
 130 temperature, water vapor, and total gas density fields for all Guillermo simulations was
 131 achieved by examining vertical profiles from ECMWF analyses obtained near the time period
 132 of the dual-Doppler radar data (1830 UTC 2 August to 0030 UTC 3 August 1997) and using a
 133 representative composite. Though some uncertainty exists within the thermodynamic fields
 134 with regard to the actual environment versus the perturbed environment obtained from the
 135 ECMWF soundings, the impact of this uncertainty was deemed to be smaller than that
 136 associated with the momentum fields, i.e., the simulated vortex is sensitive to small changes
 137 in wind shear. So to quantify this sensitivity, the horizontal velocity fields, $u^{1'}$ and $u^{2'}$, were
 138 initialized as follows

$$u^{1'}(x^{3'}) = \phi_{shear}[ecmwf_u(x^{3'}) + 1.5], \quad (3)$$

$$u^{2'}(x^{3'}) = \phi_{shear}[ecmwf_v(x^{3'}) - 1.5], \quad (4)$$

139 where ϕ_{shear} is a tuning coefficient that determines the shear impacting hurricane Guillermo
 140 within a range of 0 and 1, $x^{3'}$ is the height, and $ecmwf_u$ and $ecmwf_v$ represent mean
 141 soundings calculated from the ECMWF analyses.

142 Given the delicate balance in nature that is needed for a sheared hurricane to intensify, it
 143 is not entirely obvious whether numerical models, that are necessarily limited in resolution,
 144 can accurately represent boundary processes that are responsible for supplying water vapor
 145 to eyewall convection. The accurate representation of boundary-layer processes implies the
 146 model has been somewhat tuned to represent the impacts of waves, sea spray, and air bubbles
 147 within the water; likewise the accurate treatment of energy release in eyewall convection
 148 implies that the upward movement of, for example, moisture is being reasonably simulated
 149 by the hurricane model.

150 To examine this uncertainty the diffusion coefficient for surface momentum calculations

151 was specified as follows

$$\kappa = \kappa_{surfacefriction} \tanh\left(\frac{\mathbf{V}_h}{80}\right), \quad (5)$$

152 where $\kappa_{surfacefriction}$ is a tuning coefficient that ranges from 0.1 to 10 $\text{m}^2 \text{s}^{-1}$ and \mathbf{V}_h is the
 153 near surface horizontal wind speed. A no-slip boundary condition was utilized in the horizon-
 154 tal momentum equations ($u^{1'} = u^{2'} = 0$) with the magnitude of $\kappa_{surfacefriction}$ the determining
 155 factor with regard to the impact of this boundary condition on the intensity and structure of
 156 Guillermo. Note, unlike for the horizontal momentum equations, all scalar equations use a
 157 diffusion coefficient estimated from the *TKE* equation within calculations of surface fluxes.

158 Another uncertain boundary-layer process that has a significant impact on intensification
 159 rate is surface moisture availability and the unresolved vertical transport of this water vapor
 160 with the first term, q_v^s , being formulated as follows

$$q_v^s = q_{vs} (0.75 + q_{v_{surface}}) \tanh\left(\frac{\mathbf{V}_h}{30}\right), \quad (6)$$

161 where q_{vs} is the saturated vapor pressure over water and $q_{v_{surface}}$ is a tuning coefficient that
 162 ranges in value from 0.0 to 0.2. This term enters into surface diffusional flux calculations of
 163 water vapor, $F_{q_v}^{3'}$, in discrete form as follows

$$F_{q_v}^{3'} = \kappa \frac{q_v^1 - q_v^s}{0.5\Delta x^{3'}}, \quad (7)$$

164 where q_v^1 is the specific humidity of the first grid cell in the vertical direction. To address
 165 the uncertainty associated with the turbulent transport of water vapor (and all other fields)
 166 from the surface to the free atmosphere the turbulent length scale was modified as follows

$$L_s^m = \phi_{turb} L_s, \quad (8)$$

167 where the tuning coefficient, ϕ_{turb} , ranged from 0.1 to 10, and the eddy diffusivity now being
 168 $\kappa = 0.09 L_s^m \sqrt{TK\bar{E}}$.

169 2.A.4) DISCRETE MODEL

170 The discrete model for the Navier-Stokes equation set and the bulk microphysical model
171 closely follows what was described in section 2c of RJ. This discrete equation set formulated
172 on an A-grid can utilize a variety of time-stepping procedures with the current simulations
173 using a semi-implicit procedure (Reisner et al. (2005)). The advection scheme used to advect
174 gas and various cloud quantities was the quadratic upstream interpolation for convective
175 kinematics advection scheme including estimated streaming terms (QUICKEST, Leonard
176 and Drummond (1995)) with these quantities having the possibility of being limited by a
177 flux-corrected transport procedure (Zalesak (1979)).

178 The domain spans 1200 km in either horizontal direction and 21 km in the vertical
179 direction. The stretched horizontal mesh employing 300 grid points has the highest resolution
180 of 1 km at the center of the mesh and lowest resolution of 7 km at the model edges. Because
181 of the addition of a mean wind intended to keep the vortex centered in the middle of the
182 domain, the coarsest resolution resolving the highest wind field of Guillermo is approximately
183 2 km. The stretched vertical mesh is resolved by 86 grid points with highest resolution of
184 50 m at the surface and lowest of 500 m at the model top.

185 *2.b. Parameter estimation Model*

186 In this section the ensemble Kalman filter (EnKF) method is briefly described. In the
187 current work, the EnKF is mainly utilized to estimate the model parameters.

188 2.B.1) PARAMETER ESTIMATION WITH ENKF

189 The ensemble Kalman Filter is a Monte Carlo approach of the Kalman filter which
190 estimates the covariances between observed variables and the model state variables through
191 an ensemble of predictive model forecasts. The EnKF was first introduced by Evensen
192 (1994) and is discussed in detail in Evensen and van Leeuwen (1996) and in Houtekamer and

193 Mitchell (1998). For the current study, only the parameters will be estimated, not the state
 194 vector of the model. The EnKF procedure is directly applied to the parameters, i.e., the
 195 state vector contains only the parameter values. Nevertheless, the model covariance matrix
 196 is still required for the innovation with observations. The following EnKF description will
 197 be concern with model parameters.

198 Let $\mathbf{p} \in \mathbb{R}^\ell$ be a vector holding the different model parameters, and $\mathbf{x}^f \in \mathbb{R}^n$ be the model
 199 state forecast. Let $(\mathbf{p}_i, \mathbf{x}_i^f)$ for $i = 1 \dots N$ be an ensemble of model parameters and state
 200 forecasts, and $\mathbf{y}^o \in \mathbb{R}^m$ a vector of m observations, then the estimated parameter values \mathbf{p}_i^a
 201 given by the EnKF equations are

$$\mathbf{p}_i^a = \mathbf{p}_i + \tilde{\mathbf{K}} \left(\mathbf{y}_i^o - \mathbf{H}\mathbf{x}_i^f \right), \quad i = 1, \dots, N \quad (9)$$

$$\tilde{\mathbf{K}} = \mathbf{C}^T \mathbf{H}^T \left(\mathbf{H} \mathbf{P}^f \mathbf{H}^T + \mathbf{R} \right)^{-1}, \quad (10)$$

202 where the matrix $\tilde{\mathbf{K}} \in \mathbb{R}^{\ell \times m}$ is a modified Kalman gain matrix (see Appendix A), $\mathbf{P}^f \in \mathbb{R}^{n \times n}$
 203 is the model forecast covariance matrix, $\mathbf{C} \in \mathbb{R}^{n \times \ell}$ is the cross-correlation matrix between
 204 the model forecast and parameters, $\mathbf{R} \in \mathbb{R}^{m \times m}$ is the observations covariance matrix, and
 205 $\mathbf{H} \in \mathbb{R}^{m \times n}$ is an observation operator matrix that maps state variables onto observations.
 206 In the EnKF, the vector \mathbf{y}_i^o is a perturbed observation vector defined as

$$\mathbf{y}_i^o = \mathbf{y}^o + \varepsilon_i, \quad (11)$$

207 where $\varepsilon_i \in \mathbb{R}^m$ is a random vector sampled from a normal distribution with zero mean and a
 208 specified standard deviation σ . Usually σ is taken as the variance or error in the observations.

209 One of the main advantages of the EnKF is that the model forecast covariance matrix is
 210 approximated using the ensemble of model forecasts,

$$\mathbf{P}^f \approx \frac{1}{N-1} \sum_{i=1}^N \left(\mathbf{x}_i^f - \bar{\mathbf{x}}^f \right) \left(\mathbf{x}_i^f - \bar{\mathbf{x}}^f \right)^T, \quad (12)$$

211 where $\bar{\mathbf{x}}^f \in \mathbb{R}^n$ is the model forecast ensemble average. The use of an ensemble of model
 212 forecast to approximate \mathbf{P}^f enables the evolution of this matrix for large non-linear models

213 at a reasonable computational cost. Additionally, the cross-correlation matrix \mathbf{C} is defined
 214 as

$$\mathbf{C} = \frac{1}{N-1} \sum_{i=1}^N (\mathbf{x}_i^f - \bar{\mathbf{x}}^f) (\mathbf{p}_i - \bar{\mathbf{p}})^T, \quad (13)$$

215 where $\bar{\mathbf{p}} \in \mathbb{R}^\ell$ is the parameter ensemble average.

216 For our particular implementation, the system of equations (9)-(10) is rewritten as

$$(\mathbf{H}\mathbf{P}^f\mathbf{H}^T + \mathbf{R}) \mathbf{z}_i = (\mathbf{y}_i^o - \mathbf{H}\mathbf{x}_i^f) \quad (14)$$

$$\mathbf{p}_i^a = \mathbf{p}_i + \mathbf{C}^T\mathbf{H}^T\mathbf{z}_i, \quad (15)$$

217 for $i = 1, \dots, N$, where $\mathbf{z}_i \in \mathbb{R}^m$ is the solution of the linear system (14) for ensemble i .
 218 For our implementation, the observation covariance matrix \mathbf{R} is taken as a diagonal matrix,
 219 with σ in its main diagonal.

220 2.B.2) CONSIDERATIONS FOR PARAMETER ESTIMATION WITH ENKF

221 Several studies have utilized the EnKF data assimilation to simultaneously estimate
 222 the model state and parameter. Among them are the studies by Aksoy et al. (2006a),
 223 Aksoy et al. (2006b), Tong and Xue (2008), Hu et al. (2010), and Nielsen-Gammon et al.
 224 (2010). Typically, the parameters are included as part of the model state in the assimilation.
 225 This evolving of dynamical and non-evolving elements within the analysis introduces some
 226 difficulties for parameter estimation, such as parameter collapse and assimilation divergence.
 227 To mitigate these difficulties, the parameters are inflated to a prespecified variance, so as to
 228 avoid the collapse and keep a reasonable spread in the parameters. These techniques have
 229 proven to be effective to estimate parameter, but they require adjustments and tuning of
 230 the inflation to obtain good estimates.

231 The particular approach taken in this work is to use the EnKF as a tool to only estimate
 232 the model parameters using the available data. This approach is significantly different from
 233 the studies mentioned above in the sense that only the parameters are estimated with the
 234 EnKF, that is, the model state is not being estimated. The motivation behind this approach

235 is that model parameters are assumed to be constant, they do not evolve through the model,
 236 although they affect the dynamics of the solution. For this reason, determining parameters
 237 can be viewed as a stationary or static optimization. Our objective is to estimate a constant
 238 parameter value for the given data set, over the given time window. To achieve this, the
 239 assimilation of the data is performed on each time instance, where observations are available,
 240 independently. The reasoning behind this technique is to treat the parameters as constants
 241 and non-evolving elements in the model, hence for each time period we compute an estimated
 242 parameter value.

243 The procedure used to estimate the parameters is the following: Let t_1, \dots, t_k be the
 244 time instances where observations are available. For each time instance $t_j, j = 1, \dots, k$, the
 245 EnKF data assimilation (equations (14)-(15)) provides parameter estimates for the ensemble,
 246 $\mathbf{p}_i^a(t_j), i = 1 \dots N$. A final parameter estimate is then computed by first taking the ensemble
 247 average and then the time average of the parameters, that is

$$\mathbf{p}^a = \frac{1}{k} \sum_{j=1}^k \left[\frac{1}{N} \sum_{i=1}^N \mathbf{p}_i^a(t_j) \right] \quad (16)$$

248 One advantage is that this approach avoids the problem of parameter collapse and filter
 249 divergence, since the data assimilation is used to estimate the parameters at each time
 250 instance independently. Additionally, since the state is not being updated in the assimilation,
 251 and only the parameter are being estimated, localization is not required for the EnKF.

252 The number of available data points for Hurricane Guillermo is about 200,000 at any
 253 given time. This rich data set can be used to investigate a number of aspects of hurricane
 254 intensification. In order to exploit this data set for assimilation, we used an efficient matrix-
 255 free EnKF algorithm developed by Godinez and Moulton (in press, DOI: 10.1007/s10596-
 256 011-9268-9). The algorithm works by efficiently solving the linear system (14) using a solver
 257 based on the Sherman-Morrison formulas. In their paper, Godinez and Moulton (in press,
 258 DOI: 10.1007/s10596-011-9268-9) show that this algorithm is more efficient than traditional
 259 implementations of the EnKF, by several orders of magnitude, and enables the assimilation of
 260 vast amounts of data. Additionally, the algorithm provides an analysis that is qualitatively

261 and quantitatively the same as more traditional implementations. The reader is referred
262 to the work of Godinez and Moulton (in press, DOI: 10.1007/s10596-011-9268-9) for more
263 details.

264 **3. Parameter estimation model setup**

265 This section describes the three necessary steps to conduct the parameter estimates: the
266 processing of derived observational data fields; the setting up of the ensemble; and the setup
267 of the EnKF system.

268 *3.a. Derived Doppler data fields*

269 The primary driver of a hurricane is the release of latent heat in clouds, which arises
270 mainly from condensation. Latent heat cannot be observed directly and instruments, such
271 as Doppler radars, only measure the reflectivity and radial velocity of precipitation particles
272 averaged over the pulse volume. As a result, retrievals of dynamically relevant quantities
273 (e.g. the Cartesian wind components and latent heat) are required. Guillermo's 3-D wind
274 field was retrieved using a variational approach on a system of equations that includes the
275 radar projection equations, the anelastic mass continuity equation, and a Laplacian filter
276 (Gao et al. (1999); Reasor et al. (2009)). This wind field and estimates of the precipitation
277 water content (derived from the reflectivity measurements) are used to retrieve the latent
278 heat of condensation/evaporation following Guimond et al. (2011). There are two main
279 steps in the latent heat retrieval algorithm: (1) determine the saturation state at each grid
280 point in the radar analysis using the precipitation continuity equation; and (2) compute the
281 magnitude of heat released using the first law of thermodynamics and the vertical velocity
282 estimates described in Reasor et al. (2009). There are several potential sources of error in
283 the latent heat retrievals and a detailed treatment of these errors can be found in Guimond
284 et al. (2011). Here, we summarize the most relevant information.

285 The uncertainty in the latent heat retrievals reduces to uncertainties in two main fields:
 286 reflectivity and vertical velocity. Guimond et al. (2011) were able to reduce and/or document
 287 the uncertainty in these fields to a level where the latent heat retrievals have a reasonably
 288 acceptable accuracy. For example, Guimond et al. (2011) focus on the inner portion of the
 289 eyewall and often use two aircraft to construct the radar analyses (Reasor et al. (2009)),
 290 which reduce the effects of attenuation. In an attempt to correct the known calibration
 291 bias in the NOAA P-3 Tail radar reflectivity, 7 dB was added to the fields (John Gamache
 292 and Paul Reasor, personal communication). More importantly, however, the reflectivity is
 293 only used to determine the condition of saturation in the latent heat retrieval. Thus, the
 294 algorithm is not dependent on the precise value of the reflectivity rendering the retrievals
 295 somewhat insensitive to errors (Guimond et al. (2011)).

296 The uncertainties in the magnitude of the retrieved heating are dominated by errors in
 297 the vertical velocity. Using a combination of error propagation and Monte Carlo uncertainty
 298 techniques, biases are found to be small, and randomly distributed errors in the heating
 299 magnitudes are 16% for updrafts greater than 5 m s⁻¹ and 156% for updrafts of 1 m s⁻¹
 300 (Guimond et al. (2011)). Even though errors in the vertical velocity can lead to large
 301 uncertainties in the latent heating field for small updrafts/downdrafts, in an integrated sense,
 302 the errors are not as drastic. Figure 2 (from Guimond et al. (2011)) shows example horizontal
 303 views (averaged over all heights) of the latent heating rate of condensation/evaporation for
 304 four of the ten aircraft sampling periods of Guillermo.

305 For the assimilation, only latent heat data where there is a non-zero reflectivity value
 306 are incorporated into the data set. The errors for the retrieved wind fields are set to 5.0 to
 307 6.0%, and the errors in the retrieved latent heating, as a percentage, are specified following
 308 Guimond et al. (2011)

$$\delta \mathbf{y}_{lh}^o = \left| \frac{\delta \mathbf{w}}{\mathbf{w}} \right| \times 100 \quad (17)$$

309 where $\delta \mathbf{w} = 1.56 \text{ m s}^{-1}$ represents the overall uncertainty in the vertical wind velocity field
 310 \mathbf{w} Reasor et al. (2009). It is worth to notice that these errors are sometimes overestimated

311 or underestimated. Thus in an integral sense, the errors are not so drastic, the bias is only
 312 of $+0.16 \text{ m s}^{-1}$.

313 3.b. *Guillermo ensemble setup*

314 Since the primary goal is to examine the impact of various model parameters containing
 315 high uncertainty on the intensity and structure of Guillermo, but not the track, all simu-
 316 lations comprising the ensemble have been undertaken in which a mean wind of 1.5 m s^{-1}
 317 was added or subtracted to the respective environmental wind components to prevent the
 318 movement of Guillermo from a region containing high spatial resolution found in the domain
 319 center. Specifically this high resolution patch in Cartesian space, $\Delta x_c^{1'}$ and $\Delta x_c^{2'}$, is defined
 320 as follows

$$\Delta x_c^{1'} = 6000 \sin^2(\phi_g x^*) + 1000, \quad (18)$$

$$\Delta x_c^{2'} = 6000 \sin^2(\phi_g y^*) + 1000, \quad (19)$$

321 where $\phi_g = \frac{\pi}{N_{gp_{i'}}}$ determines how quickly the grid spacing changes from 7 km near the model
 322 edges to 1 km near the center with $N_{gp_{i'}}$ the number of grid points in either direction and
 323 x^* , y^* represent grid values for a normalized grid with a domain employing $0.5N_{gp_{i'}}$ grid
 324 points away from a center location in which $x^* = y^* = 0$. Like the horizontal direction, the
 325 vertical direction also employs stretching with highest resolution near the ocean boundary,
 326 approximately 50 m, and coarsest near the model top, 500 m, with 86 vertical grid points
 327 being utilized to resolve a domain extending upwards to 21 km. Note, because of the
 328 relatively high vertical spatial resolution, time step size was limited to 1 s to avoid any
 329 instabilities associated with exceeding the advective Courant number limit.

330 The ensemble is generated by perturbing only the four parameters discussed in Section
 331 2.a.3, which are ϕ_{shear} , $\kappa_{surfacefriction}$, $q_{v_{surface}}$, and ϕ_{turb} . The parameter values are gener-
 332 ated by the Latin hypercube sampling technique with a uniform distribution, where each
 333 parameter is sampled over a specified interval. All ensembles have the same initial, where

334 the background fields are initialized as described in Section 2.a.3, where the background
335 winds that are independent of the wind field associated with Guillermo are initialized using
336 ECMWF data. Whereas to initialize the wind field associated with Guillermo a composite
337 of the radar winds and a bogus vortex is employed within a nudging procedure over a one
338 hour time period. Afterwards, the hurricane model is simulated in free mode for five hours
339 to become balanced with the parameters, and develop a hurricane vortex. It is important to
340 mention that at this stage the behavior of the ensemble simulations are mainly dominated
341 not by the initial conditions, but by the parameter values. Hence utilizing derived fields
342 from the same hurricane for a vortex initialization does not bias the results of the parameter
343 estimation experiments, as long as the subsequent spin-up is sufficiently long to allow the
344 parameters dominate the long-term behavior of the simulation.

345 *3.c. EnKF and Observation Selection*

346 The EnKF data assimilation is used to estimate only the parameters of interest. The time
347 distribution of the parameters is obtained by assimilate each time period independently, as
348 stated in Section 2.b.2. A final parameter value is obtained by averaging in time the results
349 of the assimilation. The particular algorithm used for the parameter EnKF is a matrix-free
350 algorithm presented in Godinez and Moulton (in press, DOI: 10.1007/s10596-011-9268-9).

351 The initial set of parameter values are generated using a Latin Hypercube sampling
352 strategy with a uniform distribution. The interval for each parameter, shown in Table 1 is
353 chosen according to the values mentioned in Section 2.a, which are based on prior sensitivity
354 simulations and from a physical intuition of their interaction with the model. Figure 3 shows
355 the initial distribution for each parameter of interest.

356 Although the optimal ensemble size for estimating reliable model uncertainty is still under
357 active research, an ensemble of 120 members was deemed appropriate to capture essential
358 model statistics for parameter estimation. Upon completion of the 120 member ensemble and
359 due to the small movement of simulated hurricanes within the ensemble, information from

360 each ensemble member was independently interpolated to the center location of the grid such
 361 to be coincident with the observations. Note, only a portion of the computational domain
 362 was utilized within the EnKF corresponding to the portion of the domain that contains the
 363 derived fields of winds and latent heat. Finally, after this interpolation step, all interpolated
 364 model and derived data fields were read into the EnKF to conduct the parameter estimation
 365 for a given time period.

366 The data selection procedure followed in this paper is similar to the rank parameter-
 367 observation correlation procedure presented by Tong and Xue (2008). The parameter cross-
 368 correlation matrix, \mathbf{C} in equation (13), provides information of the correlation between the
 369 model state variables and the parameters. By applying the observation operator \mathbf{H} to the
 370 model state, we have

$$\tilde{\mathbf{C}} = \frac{1}{N-1} \sum_{i=1}^N \left(\mathbf{H}\mathbf{x}_i^f - \mathbf{H}\bar{\mathbf{x}}^f \right) (\mathbf{p}_i - \bar{\mathbf{p}})^T, \quad (20)$$

371 which is a cross-correlation matrix between parameters and model state variables in obser-
 372 vation space. The correlations are then sorted and the observational data points that are
 373 located in regions of largest correlations are selected for assimilation. It is important to note
 374 that the regions of high correlation can be identified from different model variables fields,
 375 such as latent heat, horizontal winds, or reflectivity. This enables the use one of these fields
 376 as a proxy for observation localization in order to better capture the physical processes of
 377 interest.

378 4. Results

379 This section will highlight the three main points of this paper: 1) the highly nonlinear
 380 interactions between the various parameters leading to large variations in the simulated
 381 intensity and structure of Guillermo among the 120 ensemble members; 2) the large amounts
 382 of derived data, horizontal winds or latent heat, required to reasonably estimate the four
 383 model parameters; and 3) the newly estimated parameters lead to an overall reduction in

384 the model forecast error.

385 *4.a. Ensemble spread and structure*

386 Since the EnKF method depends on proper model statistics to optimally determine the
387 parameter values (Anderson (2001)) this section will illustrate this necessary variability
388 across the various members of the ensemble. Likewise, for reasonable parameter estimation
389 it is important that the ensemble produces statistics that are within the range of the ob-
390 servations and this is another aspect of the ensemble that will be presented. For example,
391 Fig. 4 shows the simulated pressure traces for the 120 ensemble members (blue lines), the
392 ensemble average (black line), and the 3-hourly observations from the NHC advisories (red
393 dots) with a large spread in hurricane intensity being denoted within the ensemble. Further,
394 even though this result may be somewhat fortuitous, the ensemble-averaged pressure trace
395 is in remarkably good agreement with observations with a difference less than 5 hPa. To
396 highlight differences between the ensemble average and a given member, in addition to dis-
397 playing ensemble average statistics, results from a select ensemble member, i.e., member 44,
398 that also reasonably reproduced the observed pressure trace will be shown.

399 Because hurricane Guillermo was embedded in an environment characterized with vertical
400 wind speed shear, its observed eyewall horizontal structure was asymmetric with a dominant
401 wavenumber 1 mode, e.g., Reasor et al. (2009) and Sitkowski and Barnes (2009). To illustrate
402 the models ability to reproduce this asymmetry Fig. 5 shows both the ensemble-averaged
403 layer-averaged vertical velocities and the corresponding layer-averaged fields from member 44
404 at two different layers. As evident in this figure, the vortex in both the average sense and
405 for member 44 is asymmetric with a dominant wavenumber 1 mode being readily apparent.
406 Likewise, the impact of averaging across all members is clearly evident in Fig. 5 with a
407 significant smoothing and reduction in vertical motions being noted with regard to the
408 vertical motion fields produced by ensemble member 44. Furthermore, using a similar Fourier
409 spectral decomposition procedure as Reasor et al. (2009) Fig. 6 reveals significant amounts

410 of the vertical motion fields being in wavenumber 0 and 1 components with the magnitude
411 of the wavenumber 1 vertical motion field from ensemble member 44 reasonably agreeing
412 with the observations (see Fig. 15a of Reasor et al. (2009)).

413 To provide another view of the simulated storm structure, both the ensemble averaged
414 and ensemble 44 azimuthal structures were compared to observations and are presented for
415 two flight legs in Figs. 7-8. Common disagreement with observations can be seen in both
416 figures: First the simulated radius of maximum wind (RMW) and hence eyewall size is
417 about 5 – 10 km smaller than in the observations. While the simulated ensemble averaged
418 azimuthal tangential component of the wind lies within $\sim 10 \text{ m s}^{-1}$ of the observations,
419 more notable differences are seen in the radial component of the wind with magnitudes
420 rarely exceeding 10 m s^{-1} in the observations and the simulation consistently producing
421 magnitudes exceeding 15 m s^{-1} . Similar overestimation is produced in the latent heat fields,
422 with values exceeding 25 or even 30 (1000 K h^{-1}) in the simulation with the observations
423 showing values marginally reaching 20 (1000 K h^{-1}).

424 Despite these noteworthy differences, the HIGRAD model is able to reproduce the
425 slope/tilt of radial, tangential and latent heat fields with a reasonable degree of realism.
426 Moreover, the heights above sea level of the contours encompassing the largest simulated
427 values of those three fields are in overall good agreement with observations. Note, that the
428 larger values of latent heat are required to compensate for the impact of spurious evaporation
429 (Reisner and Jeffery (2009)) common to most cloud models with the consequences of this
430 evaporation being discussed later in this manuscript. Additional plots were made for the
431 remaining 8 flight legs (not shown) and displayed similar attributes.

432 *4.b. Twin-Experiments for Parameter Estimation*

433 To assess the reliability of parameter estimation within the current context, and the
434 amount of observational data needed for the estimation, a series of twin-experiments were
435 performed. A synthetic observational data set is produced from a reference model run with

436 the specific parameter values give in Table 2, and initialized according to Section 3.b. These
437 reference parameters were selected near the ensemble average with white noise added to
438 them.

439 In their paper Tong and Xue (2008) found that to simultaneously estimate the model
440 state and five parameters with the ensemble square root filter, using their rank parameter-
441 observation procedure, they needed only 30 observational data points. Given that our pa-
442 rameter estimation setting is significantly different from their approach, it is not entirely
443 obvious whether only small amounts of data are required to conduct the parameter estima-
444 tion or, in the other limiting situation, more data than is currently available is needed for
445 undertaking the estimates. To address this issue, nine parameter estimation experiments,
446 named TE1 to TE9, were performed for different amounts of data, given in Table 3. The
447 data being used for parameter estimation is the latent heat field from the reference run,
448 where the data is selected according to the procedure described in Section 3.c. The first
449 observation set was taken at $t = 6$ hours of simulation time, afterwards nine more observa-
450 tion sets were taken at 30 minute intervals, which makes a total of 10 observational data set
451 over a five hour window. For each experiment, the parameters are estimated according to
452 Section 2.b.2, that is, parameter estimates for the ensemble are computed with the EnKF at
453 each observational time, and then a final parameter estimate is then computed by averaging
454 over ensemble and then time, as in equation (16). Figure 9 shows the parameter estimates
455 for each experiment, where the vertical lines indicate the time variance of the parameter
456 estimate. The figure clearly shows the impact of the additional data on the parameter esti-
457 mates with a noticeable reduction in the error for all for parameters. Furthermore, it is only
458 when approximately 200,000 observations are used that all four parameters converge to the
459 correct values. This is highly relevant since it indicates that a significant amount of data
460 is required, in this context, to correctly estimate the values of the parameters. A similar
461 result was obtained when the horizontal wind field or reflectivity were used to estimate the
462 parameters.

464 Given the large ensemble spread in various model fields, such as intensity, and the ability
465 of the model to reproduce observed data suggests that estimation of the four model pa-
466 rameters is not only possible with the EnKF, but should produce parameter estimates that
467 hopefully reduce model forecast errors.

468 The number of observations used for parameter estimation, using the EnKF in all sub-
469 sequent experiment, were those identified with the highest ensemble sensitivity located at
470 200,000 model grid-points (see selection of observations in Section 3.c). The assimilation
471 is performed over latent heat (DA1), horizontal winds (DA2), or both fields (DA3) started
472 six hours into the ensemble (corresponding to 1900 UTC). With the inclusion of DA3, an
473 assessment regarding how the EnKF procedure weights two different observational data sets
474 and model results can be made and analyzed. Hence, this section will not only highlight
475 how the various parameter estimates change when using different observational fields, but
476 also how these estimates change in time.

477 Figure 10 shows the time distribution of the ensemble average parameter estimates with
478 EnKF using the 10 data time periods for DA1, DA2, and DA3. The largest temporal
479 oscillations in the parameter estimates are associated with DA2 and suggest that the wind
480 fields produced by the ensemble tend to oscillate more in time than the latent heat fields.
481 Likewise, the surface moisture and the wind shear parameter estimates do not appear to
482 change significantly in time, whereas the turbulent length scale and surface friction estimates
483 either increase or decrease with time. Note, the temporal changes in these two parameters
484 could be due to numerical errors and/or the impact of initial condition errors. For example,
485 Fig. 7 shows that with time the areas of maximum latent heating and/or winds from the
486 ensemble are expanding outward and hence this outward expansion, probably the result of
487 numerical diffusion, could explain the temporal changes in these two parameter estimates.

488 Upon averaging the parameter estimates over the ensemble and in time, differences be-
489 tween the various parameter values are small; however, as will be shown in the next section

490 these small differences in the parameters do lead to rather significant differences in both the
491 structure and intensity of the simulated hurricanes. Table 4 show the time average parameter
492 values from the assimilation experiments, as well as the parameter values used for ensemble
493 member 44 prior to assimilation. Fig. 11 also reveals the various parameter estimates are
494 different than the parameter values used in ensemble member 44, suggesting the importance
495 of using a technique such as the EnKF to obtain the estimates, instead of simply using
496 estimates obtained from a simulation that matches an observable such as minimum sea level
497 pressure. This ability of the EnKF to reasonably fit the parameter values to the chosen
498 observational data set is as well illustrated by the time averaged estimates from DA3 that,
499 as expected, lie somewhere between the parameter estimates from DA1 and DA2, except for
500 the turbulent length scale parameter.

501 *4.d. Parameter error assessment*

502 To illustrate the ability of the parameter estimates to reduce model forecast error, three
503 simulations (SDA1, SDA2, and SDA3) were run using the time average parameter estimates
504 from DA1, DA2, and DA3 shown in table 4. The setup for each simulation is the same
505 as described in Subsection 3.b. Both qualitatively (see Figs. 12-13) and quantitatively (see
506 Fig. 14) the parameter estimates produce model fields that are in better agreement with
507 observed fields, especially the estimates associated with DA1 or those derived from using
508 the latent heat fields. Though it is not surprising that SDA1 best matches the observed
509 latent heat fields, what was surprising was the errors associated with the wind fields were
510 lower in SDA1 than those associated with SDA2. This suggests the possible utility of using
511 latent heat instead of more traditional observational fields such as horizontal winds or radar
512 reflectivity within data assimilation procedures to estimate model parameters and/or por-
513 tions of the model state vector. When a combination of both observational fields are utilized
514 for parameter estimation, error estimates from SDA3 reveal that the response is weighted
515 towards producing results closer to SDA2, suggesting the dominance of the horizontal wind

516 observational data in the parameter estimates. This behavior can also be appreciated in the
517 parameter estimates themselves, as seen in Figs. 10 and 11.

518 Though Fig. 14 demonstrates that SDA1 produces lower errors than SDA2 and SDA3,
519 Fig. 15 illustrates that the intensity of SDA1 is significantly weaker than SDA3 and slightly
520 weaker than SDA2. This finding may suggest that in order for SDA1 to accurately reproduce
521 the intensity of Guillermo additional observational data is needed below the range of the
522 radar (approximately 1 km in height) or that other errors, such as numerical errors, are
523 contributing to the intensity differences, i.e., numerical diffusion and spurious evaporation
524 associated with large numerical errors found near cloud boundaries. Note, like ensemble
525 member 44, SDA2 produces nearly twice the observed amount of latent heat (see Fig. 13)
526 suggesting the simulation is indeed having to compensate for large amounts of spurious
527 evaporative cooling.

528 For example, the bottom panels of Figs. 12-13 show areas of evaporative cooling occurring
529 immediately to the left of regions of strong positive latent heat release that do not have an
530 analog in the observed fields. Hence, similar to what is shown in Fig. 3b of Margolin et al.
531 (1995), this spurious cooling appears to be the result of not being able to resolve the sub-
532 grid movement of cloud boundaries, i.e., the so-called advection-condensation problem. In
533 fact, when a simulation using the evaporative limiter described in Reisner and Jeffery (2009)
534 along with the parameter values from DA1 is run the resulting minimum sea level pressure
535 from this simulation is actually slightly lower than the observed pressure (not shown). But,
536 though SDA1 appears to suffer from relatively large numerical errors that are also common to
537 all hurricane models, the end result of the parameter estimation procedure is still a reduction
538 in overall model forecast error.

539 5. Summary and conclusions

540 This paper presented the estimation of key model parameters found within a hurricane
541 model, through the use of EnKF data assimilation. The particular approach taken was to
542 use the EnKF to only estimate the parameters at each time instance where observations
543 were available. The advantage of this approach is that it avoids the combination of dynamic
544 and non-dynamic elements in the assimilation procedure, which introduces difficulties when
545 estimating parameters. An efficient matrix-free EnKF data assimilation algorithm Godinez
546 and Moulton (in press, DOI: 10.1007/s10596-011-9268-9) is used to assimilate the derived
547 data fields; namely horizontal wind or latent heat, available for Hurricane Guillermo. Like-
548 wise, upon completion of a 120 member ensemble that reasonably reproduced observations,
549 the parameter estimation experiments show that a large number of data points are indeed
550 required within the current approach to provide a reasonable estimate of the model parame-
551 ters. Nevertheless, the parameter estimation procedure presented in this work can be easily
552 be applied to other models and data sets.

553 A unique aspect of this work was the utilization of derived fields of latent heat to estimate
554 the parameters. The estimates obtained using these derived fields produced lower model
555 forecast errors than a simulation using parameter estimates obtained from horizontal wind
556 fields or radar reflectivity alone (not shown). Unlike latent heat which can be directly
557 linked to a simple physical process occurring within a hurricane model, i.e., condensation,
558 utilization of other data fields such as radar reflectivity require the model to faithfully capture
559 physical processes that are not yet well understood, i.e. collision-coalescence; and are also
560 not the primary driver for hurricane intensification, potentially leading to large errors in
561 parameter estimates. This result also suggests the parameters associated with the primary
562 component of hurricane intensification, condensation of water vapor into cloud water, should
563 also be included in the current parameter estimation procedure. It is important to note that
564 deriving latent heat fields requires accurate vertical velocity measurements, which in most
565 cases are not available. The availability of dual-Doppler radar data, for Hurricane Guillermo,

566 made the computation of latent heat possible. Such a data set might not be easily acquired
567 for other hurricanes, but one of the contributions of this work is to demonstrate the value of
568 such a data set for parameter estimation.

569 Another subtle aspect suggested by this paper is that in order for a given hurricane
570 model to both reproduce a realistic latent heat field and the correct intensity, numerical
571 errors, especially near cloud edges, must be small. Currently, all hurricane models produce
572 large numerical errors near cloud boundaries with these errors possibly inducing significant
573 amounts of spurious evaporation. Hence, future work is needed to help reduce the impact
574 of cloud-edge errors either via the calibration of a tuning coefficient employed within an
575 evaporative limiter, i.e., see Eq. A24 in Reisner and Jeffery (2009), using the current EnKF
576 procedure or replacing Eulerian cloud modeling approaches with a potentially more accurate
577 Lagrangian approach (Andrejczuk et al. (2008)).

578 *Acknowledgments.* This work was supported by the Laboratory Directed Research and De-
579 velopment Program of Los Alamos National Laboratory, which is under the auspices of the
580 National Nuclear Security Administration of the U.S. Department of Energy under DOE
581 Contracts W-7405-ENG-36 and LA-UR-10-04291. Computer resources were provided both
582 by the Computing Division at Los Alamos and the Oak Ridge National Laboratory Cray
583 clusters. Approved for public release, LA-UR-11-10121.

584 APPENDIX

585

586 **Appendix A: EnKF equations for parameter estimation**

587 Many studies have used the EnKF data assimilation to simultaneously estimate model
588 state and parameters. This can be achieved by using an augmented state vector where the
589 parameters are appended at the end of the vector. In this appendix we review the EnKF

590 equations for the simultaneous state and parameter estimation and extract the necessary
 591 equations for parameter estimation.

592 Let $\mathbf{p} \in \mathbb{R}^\ell$ be a vector holding the model parameters, and $\mathbf{x}^f \in \mathbb{R}^n$ be the model state
 593 forecast. Define the augmented state vector

$$\mathbf{w} = \begin{bmatrix} \mathbf{x}^f \\ \mathbf{p} \end{bmatrix} \in \mathbb{R}^{n+\ell} \quad (\text{A1})$$

594 and let \mathbf{w}_i for $i = 1 \dots N$ be an ensemble of model state forecast and parameters. For a
 595 vector of m observations $\mathbf{y}^o \in \mathbb{R}^m$ the EnKF analysis equations are given by

$$\mathbf{w}_i^a = \mathbf{w}_i + \tilde{\mathbf{K}} \left(\mathbf{y}_i^o - \mathbf{H}\mathbf{x}_i^f \right), \quad i = 1, \dots, N \quad (\text{A2})$$

$$\tilde{\mathbf{K}} = \begin{bmatrix} \mathbf{P}^f & \mathbf{C} \\ \mathbf{C}^T & \mathbf{B} \end{bmatrix} \begin{bmatrix} \mathbf{H}^T \\ \mathbf{0} \end{bmatrix} (\mathbf{H}\mathbf{P}^f\mathbf{H}^T + \mathbf{R})^{-1}, \quad (\text{A3})$$

596 where $\mathbf{P}^f \in \mathbb{R}^{n \times n}$ is the model forecast covariance matrix, $\mathbf{B} \in \mathbb{R}^{\ell \times \ell}$ is the parameter co-
 597 variance matrix, $\mathbf{C} \in \mathbb{R}^{n \times \ell}$ is the cross-correlation matrix between the model forecast and
 598 parameters, $\mathbf{R} \in \mathbb{R}^{m \times m}$ is the observations covariance matrix, $\mathbf{H} \in \mathbb{R}^{m \times n}$ is an observa-
 599 tion operator matrix that maps state variables onto observations, and \mathbf{y}_i^o is a perturbed
 600 observation vector. The parameter correlation matrix is given by

$$\mathbf{B} = \frac{1}{N-1} \sum_{i=1}^N (\mathbf{p}_i - \bar{\mathbf{p}}) (\mathbf{p}_i - \bar{\mathbf{p}})^T, \quad (\text{A4})$$

601 and the cross-correlation matrix is give by

$$\mathbf{C} = \frac{1}{N-1} \sum_{i=1}^N \left(\mathbf{x}_i^f - \bar{\mathbf{x}}^f \right) (\mathbf{p}_i - \bar{\mathbf{p}})^T, \quad (\text{A5})$$

602 where $\bar{\mathbf{x}}^f$ and $\bar{\mathbf{p}}$ are the ensemble average of the model forecast and parameters, respectively.

603 The system of equations (A2)-(A3) can be written as

$$(\mathbf{H}\mathbf{P}^f\mathbf{H}^T + \mathbf{R}) \mathbf{z}_i = \left(\mathbf{y}_i^o - \mathbf{H}\mathbf{x}_i^f \right) \quad (\text{A6})$$

$$\mathbf{w}_i^a = \mathbf{w}_i + \begin{bmatrix} \mathbf{P}^f & \mathbf{C} \\ \mathbf{C}^T & \mathbf{B} \end{bmatrix} \begin{bmatrix} \mathbf{H}^T \\ \mathbf{0} \end{bmatrix} \mathbf{z}_i, \quad (\text{A7})$$

604 where the vector $\mathbf{z}_i \in \mathbb{R}^m$ is the solution of equation (A6). The augmented matrix in equation
 605 (A7) can be simplified as

$$606 \quad \begin{bmatrix} \mathbf{P}^f & \mathbf{C} \\ \mathbf{C}^T & \mathbf{B} \end{bmatrix} \begin{bmatrix} \mathbf{H}^T \\ \mathbf{0} \end{bmatrix} = \begin{bmatrix} \mathbf{P}^f \mathbf{H}^T \\ \mathbf{C}^T \mathbf{H}^T \end{bmatrix},$$

607 so we have the following analysis update equations for the model forecast and parameters:

$$\mathbf{x}_i^a = \mathbf{x}_i^f + \mathbf{P}^f \mathbf{H}^T \mathbf{z}_i, \quad (\text{A8})$$

$$\mathbf{p}_i^a = \mathbf{p}_i + \mathbf{C}^T \mathbf{H}^T \mathbf{z}_i. \quad (\text{A9})$$

608 The update equation (A9), together with equations (A5) and (A6), form a system that
 609 estimate the model parameters for a given data set. This is the system used in our current
 610 study.

REFERENCES

- 613 Aksoy, A., F. Zhang, and J. Nielsen-Gammon, 2006a: Ensemble-Based Simultaneous State
614 and Parameter Estimation in a Two-Dimensional Sea-Breeze Model. *Mon. Wea. Rev.*,
615 **134**, 2951–2970.
- 616 Aksoy, A., F. Zhang, and J. Nielsen-Gammon, 2006b: Ensemble-based simultaneous state
617 and parameter estimation with MM5. *Geophys. Res. Lett.*, **33**, L12 801.
- 618 Anderson, J., 2001: An ensemble adjustment Kalman filter for data assimilation. *Mon. Wea.*
619 *Rev.*, **129**, 2884–2903.
- 620 Andrejczuk, M., J. Reisner, B. Henson, M. Dubey, and C. Jeffery, 2008: The potential
621 impacts of pollution on a non-drizzling stratus deck: Does aerosol number matter more
622 than type? *J. Geophys. Res.*, **113**, D19 204,doi:10.1029.
- 623 Annan, J. D., J. C. Hargreaves, N. R. Edwards, and R. Marsh, 2005: Parameter estimation
624 in an intermediate complexity earth system model using an ensemble Kalman filter. *Ocean*
625 *Modelling*, **8**, 135 – 154.
- 626 Evensen, G., 1994: Sequential data assimilation with a nonlinear quasi-geostrophic model
627 using Monte Carlo methods to forecast error statistics. *J. Geophys. Res.*, **99 (C5)**, 10 143–
628 10 162.
- 629 Evensen, G. and P. van Leeuwen, 1996: Assimilation of Geosat altimeter data for the Agulhas
630 Current using the ensemble Kalman filter with a quasigeostrophic model. *Mon. Wea. Rev.*,
631 **124**, 85–96.
- 632 Gao, J., M. Xue, A. Shapiro, and K. Droegemeier, 1999: A variational method for the

633 analysis of three-dimensional wind fields from two doppler radars. *Mon. Wea. Rev.*, **127**,
634 2128–2142.

635 Godinez, H. and J. Moulton, in press, DOI: 10.1007/s10596-011-9268-9: An efficient matrix-
636 free algorithm for the ensemble Kalman filter. *Comput. Geosci.*

637 Guimond, S., M. Bourassa, and P. Reasor, 2011: A Latent Heat Retrieval and Its Effects on
638 the Intensity and Structure Change of Hurricane Guillermo (1997). Part I: The Algorithm
639 and Observations. *J. Atmos. Sci.*, **68**, 1549–1567.

640 Hacker, J. P. and C. Snyder, 2005: Ensemble Kalman Filter Assimilation of Fixed Screen-
641 Height Observations in a Parameterized PBL. *Mon. Wea. Rev.*, **133**, 3260–3275.

642 Houtekamer, P. and H. Mitchell, 1998: Data assimilation using an ensemble Kalman filter
643 technique. *Mon. Wea. Rev.*, **126**, 796–811.

644 Hu, X., F. Zhang, and J. Nielsen-Gammon, 2010: Ensemble-based simultaneous state and
645 parameter estimation for treatment of mesoscale model error: A real-data study. *Geophys.*
646 *Res. Lett.*, **37**, L08 802.

647 Leonard, B. and J. Drummond, 1995: Why you should not use ‘hybrid’, ‘power-law’ or
648 related exponential schemes for convective modeling- there are better alternatives. *Int. J.*
649 *Num. Meth. Fluids*, **20**, 421–442.

650 Margolin, L., J. Reisner, and P. Smolarkiewicz, 1995: Application of the volume of fluid
651 method to the advection-condensation problem. *Mon. Wea. Rev.*, **125**, 2265–2273.

652 McFarquhar, G. and R. Black, 2004: Observations of particle size and phase in tropical
653 cyclones: Implications for mesoscale modeling of microphysical processes. *J. Atmos. Sci.*,
654 **61**, 777–794.

655 Nielsen-Gammon, J., X. Hu, F. Zhang, and J. Pleim, 2010: Evaluation of planetary boundary

656 layer scheme sensitivities for the purpose of parameter estimation. *Mon. Wea. Rev.*, **138**,
657 3400–3417.

658 Reasor, P., M. Eastin, and J. Gamache, 2009: Rapidly intensifying Hurricane Guillermo
659 (1997). Part I: Low-wavenumber structure and evolution. *Mon. Wea. Rev.*, **137**, 603–631.

660 Reisner, J. and C. Jeffery, 2009: A smooth cloud model. *Mon. Wea. Rev.*, **137**, 1825–1843.

661 Reisner, J., A. Mousseau, A. Wyszogrodzki, and D. Knoll, 2005: An implicitly balanced
662 hurricane model with physics-based preconditioning. *Mon. Wea. Rev.*, **133**, 1003–1022.

663 Sitkowski, M. and G. Barnes, 2009: Low-level thermodynamic, kinematic, and reflectivity
664 fields of Hurricane Guillermo (1997) during rapid intensification. *Mon. Wea. Rev.*, **137**,
665 645–663.

666 Thompson, G., R. Rasmussen, and K. Manning, 2008: Explicit forecasts of winter precipita-
667 tion using an improved bulk microphysics scheme. part ii: Implementation of a new snow
668 parameterization. *Mon. Wea. Rev.*, **136**, 5095–5115.

669 Tong, M. and M. Xue, 2008: Simultaneous Estimation of Microphysical Parameters and
670 Atmospheric State with Simulated Radar Data and Ensemble Square Root Kalman Filter.
671 Part II: Parameter Estimation Experiments. *Mon. Wea. Rev.*, **136**, 1649–1668.

672 Torn, R. D. and G. J. Hakim, 2009: Ensemble Data Assimilation Applied to RAINEX
673 Observations of Hurricane Katrina (2005). *Monthly Weather Review*, **137**, 2817–2829.

674 Zalesak, S., 1979: Fully multidimensional flux-corrected transport algorithm for fluids. *J.*
675 *Comput. Phys.*, **31**, 335–362.

676 Zhang, F., Y. Weng, J. Sippel, Z. Meng, and C. Bishop, 2009: Cloud-resolving hurricane
677 initialization and prediction through assimilation of Doppler radar observations with an
678 ensemble Kalman filter. *Mon. Wea. Rev.*, **137**, 2105–2125.

679 Zou, X., Y. Wu, and P. S. Ray, 2010: Verification of a High-Resolution Model Forecast Using
680 Airborne Doppler Radar Analysis during the Rapid Intensification of Hurricane Guillermo.
681 *J. Appl. Meteor. Climatol.*, **49**, 807–820.

682 List of Tables

683	1	Initial parameter intervals for sampling with Latin Hypercube strategy using	
684		a uniform distribution.	32
685	2	Parameter values used for the reference run, from where synthetic data is used	
686		for the twin-experiments.	33
687	3	Number of observations used in the twin-experiments for parameter estimation.	34
688	4	Time average parameter values for each of the experiments DA1-DA3, and	
689		the parameter values for ensemble member 44 (HG 44).	35

parameter	interval
surface moisture	[0.05, 0.2]
wind shear	[0.1, 1.0]
turbulent length scale	[0.1, 10.0]
surface friction	[0.1, 10.0]

TABLE 1. Initial parameter intervals for sampling with Latin Hypercube strategy using a uniform distribution.

parameter	value
surface moisture	9.325522e-02
wind shear	4.968604e-01
turbulent length scale	3.753693
surface friction	1.443062

TABLE 2. Parameter values used for the reference run, from where synthetic data is used for the twin-experiments.

experiment	No. obs (m)
TE1	20
TE2	63
TE3	200
TE4	632
TE5	2000
TE6	6325
TE7	20000
TE8	63246
TE9	200000

TABLE 3. Number of observations used in the twin-experiments for parameter estimation.

parameter/simulation or DA	HG 44	DA1	DA2	DA3
surface moisture	1.944818e-01	9.431537e-02	1.189942e-01	1.132110e-01
wind shear	8.122108e-01	4.843292e-01	5.744430e-01	5.506012e-01
turbulent length scale	4.524457	3.753072	4.271998	4.401512
surface friction	2.005939	1.619931	2.120377	1.986076

TABLE 4. Time average parameter values for each of the experiments DA1-DA3, and the parameter values for ensemble member 44 (HG 44).

690 List of Figures

- 691 1 Best Track for Hurricane Guillermo (1997). Hurricane Intensity is color-coded
692 based on the Saffir-Simpson scale with legend shown on the bottom left of the
693 figure. Data courtesy of the Tropical Prediction Center (TPC), NOAA. The
694 EnKF analysis period is denoted by the small black rectangle. 39
- 695 2 Horizontal views (averaged over all heights) of the latent heating rate (K h^{-1})
696 of condensation/evaporation retrieved from airborne Doppler radar observa-
697 tions in Hurricane Guillermo (1997) at four select times of the dual-Doppler
698 radar data, i.e., pass 5 corresponds to 2117 UTC from Fig. 6 of Reasor et al.
699 (2009). Note that grid points without latent heating were assigned zero values
700 after the vertical averaging. The vertical profile of the azimuthal mean latent
701 heating rate at the RMW (30 km) is shown above each contour plot. The first
702 level of data is at 1 km due to ocean surface contamination. 40
- 703 3 The parameter spread of the 120 ensemble members obtained by utilization
704 of the Latin Hypercube sampling strategy within the limits shown in Table 1 41
- 705 4 Minimum sea level pressure versus simulation time for each ensemble member
706 (blue line), ensemble average (black line), and observations (red dots), for
707 ensemble 1-30 (top left), ensemble 31-60 (top right), ensemble 61-90 (bottom
708 left), and ensemble 91-120 (bottom right). 42
- 709 5 Ensemble average vertical motion fields at 2300 UTC (11 hours into the sim-
710 ulations) averaged between 1-3 km (a) or 5-7 km (c). Corresponding layer-
711 averaged vertical motions fields from ensemble member 44 between 1-3 km
712 (b) or 5-7 km (d). 43

713	6	Time-averaged axisymmetric (black solid line) and azimuthal wavenumber-	
714		14 amplitudes of vertical velocity in the 13-km layer within a 200 km radial	
715		distance from the storm center from the ensemble average (left figure) or	
716		ensemble 44 (right figure). The averaging times are between 2230 UTC and	
717		2300 UTC.	44
718	7	Comparisons between azimuthally-averaged profiles for the ensemble average	
719		(contours) and observations (shaded) for tangential winds (top), radial winds	
720		(center), and latent heat (bottom). Time periods for comparisons are at flight	
721		leg 5 (2117 UTC) and 9 (2333 UTC).	45
722	8	Comparisons between azimuthally-averaged profiles for ensemble member 44	
723		(contours) and observations (shaded) for tangential winds (top), radial winds	
724		(center), and latent heat (bottom). Time periods for comparisons are the	
725		same as in the previous figure.	46
726	9	EnKF parameter estimation as a function of number of latent heat observa-	
727		tions assimilated. The latent heat observations were added in locations were	
728		the ensemble is most sensitive to changes in the parameters (Section 3.c).	47
729	10	Time distribution of the ensemble average parameter estimates with EnKF	
730		from DA1 (blue line, latent heat), DA2 (red line, horizontal winds), and DA3	
731		(green line, both latent heat and horizontal winds).	48
732	11	Analysis parameters averaged over time for ensemble member 44 (HG 44),	
733		DA1, DA2, and DA3. The vertical lines from the dots indicate the time	
734		variance of the parameter estimates each experiment.	49
735	12	Comparisons of the azimuthally-averaged profiles between a model simula-	
736		tion (contours) using estimated parameters from DA1 and observations (color	
737		shaded). Plots for tangential winds (top), radial winds (center), and latent	
738		heat (bottom) for flight leg 5 (2117 UTC) and 9 (2333 UTC).	50

739	13	Comparisons of the azimuthally-averaged profiles between a model simulation	
740		using estimated parameters from DA2 and observations (color shaded). Plots	
741		for tangential winds (top), radial winds (center), and latent heat (bottom) for	
742		the same time periods as in the previous figure.	51
743	14	Error estimates as a function of time computed using Eq. 20 of Reisner and	
744		Jeffery (2009) for ensemble member 44 (HG 44), SDA1, SDA2, and SDA3.	52
745	15	Minimum sea level pressure for SDA1, SDA2, and SDA3 along with the ob-	
746		served pressure from Hurricane Guillermo.	53

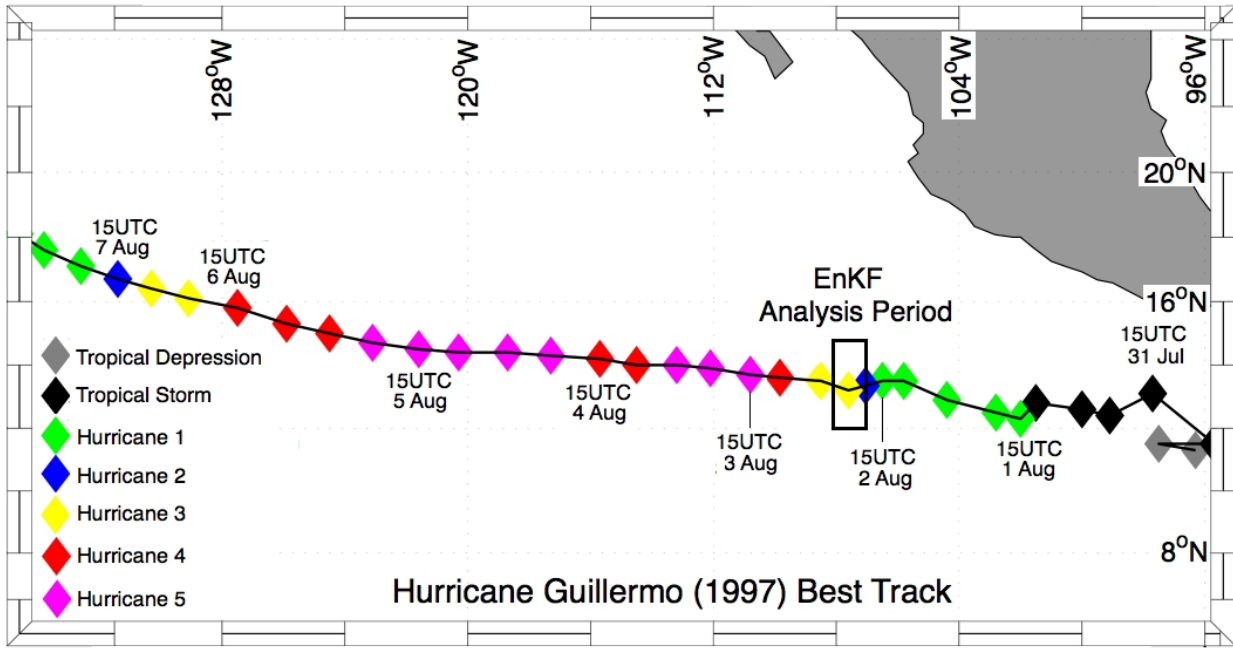


FIG. 1. Best Track for Hurricane Guillermo (1997). Hurricane Intensity is color-coded based on the Saffir-Simpson scale with legend shown on the bottom left of the figure. Data courtesy of the Tropical Prediction Center (TPC), NOAA. The EnKF analysis period is denoted by the small black rectangle.

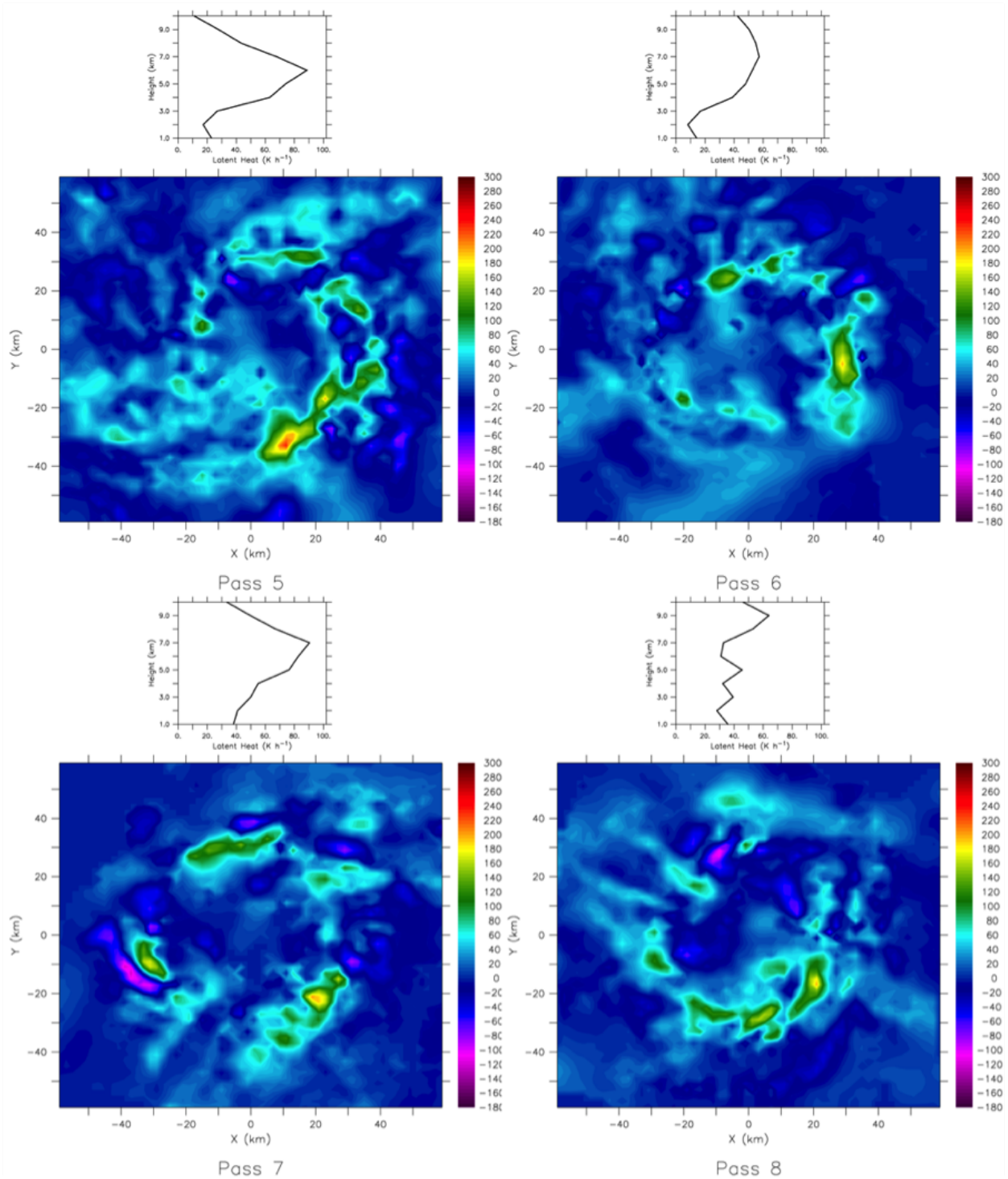


FIG. 2. Horizontal views (averaged over all heights) of the latent heating rate (K h^{-1}) of condensation/evaporation retrieved from airborne Doppler radar observations in Hurricane Guillermo (1997) at four select times of the dual-Doppler radar data, i.e., pass 5 corresponds to 2117 UTC from Fig. 6 of Reasor et al. (2009). Note that grid points without latent heating were assigned zero values after the vertical averaging. The vertical profile of the azimuthal mean latent heating rate at the RMW (30 km) is shown above each contour plot. The first level of data is at 1 km due to ocean surface contamination.

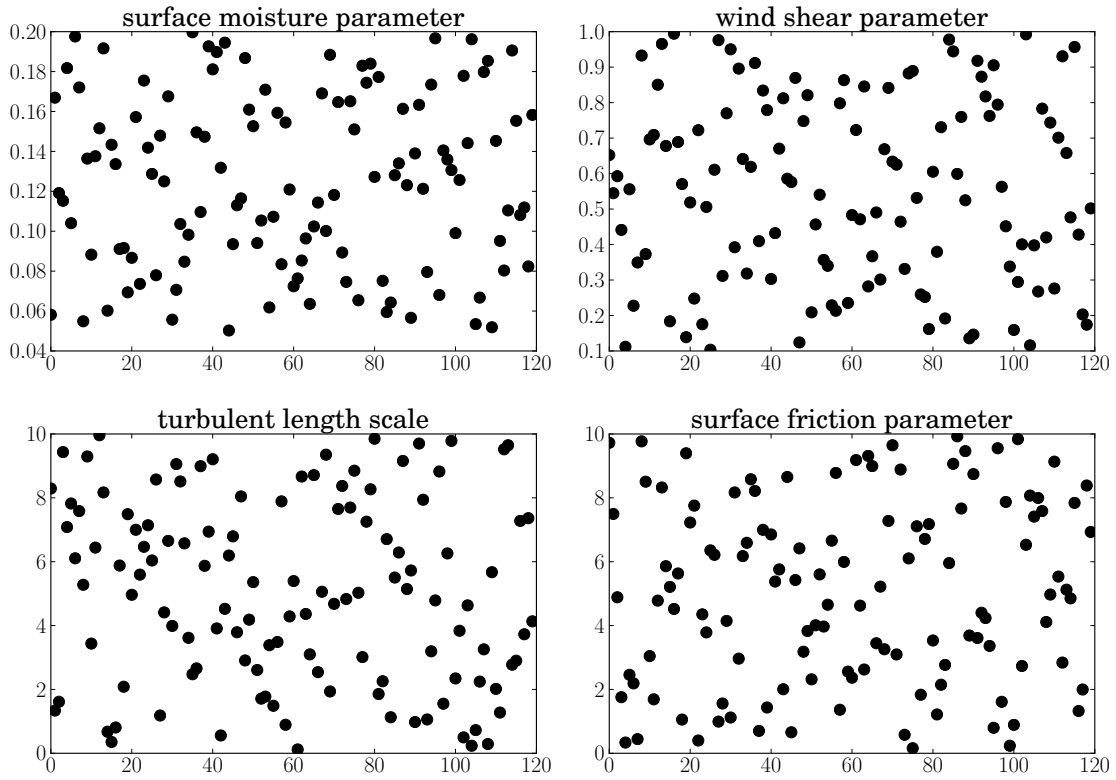


FIG. 3. The parameter spread of the 120 ensemble members obtained by utilization of the Latin Hypercube sampling strategy within the limits shown in Table 1

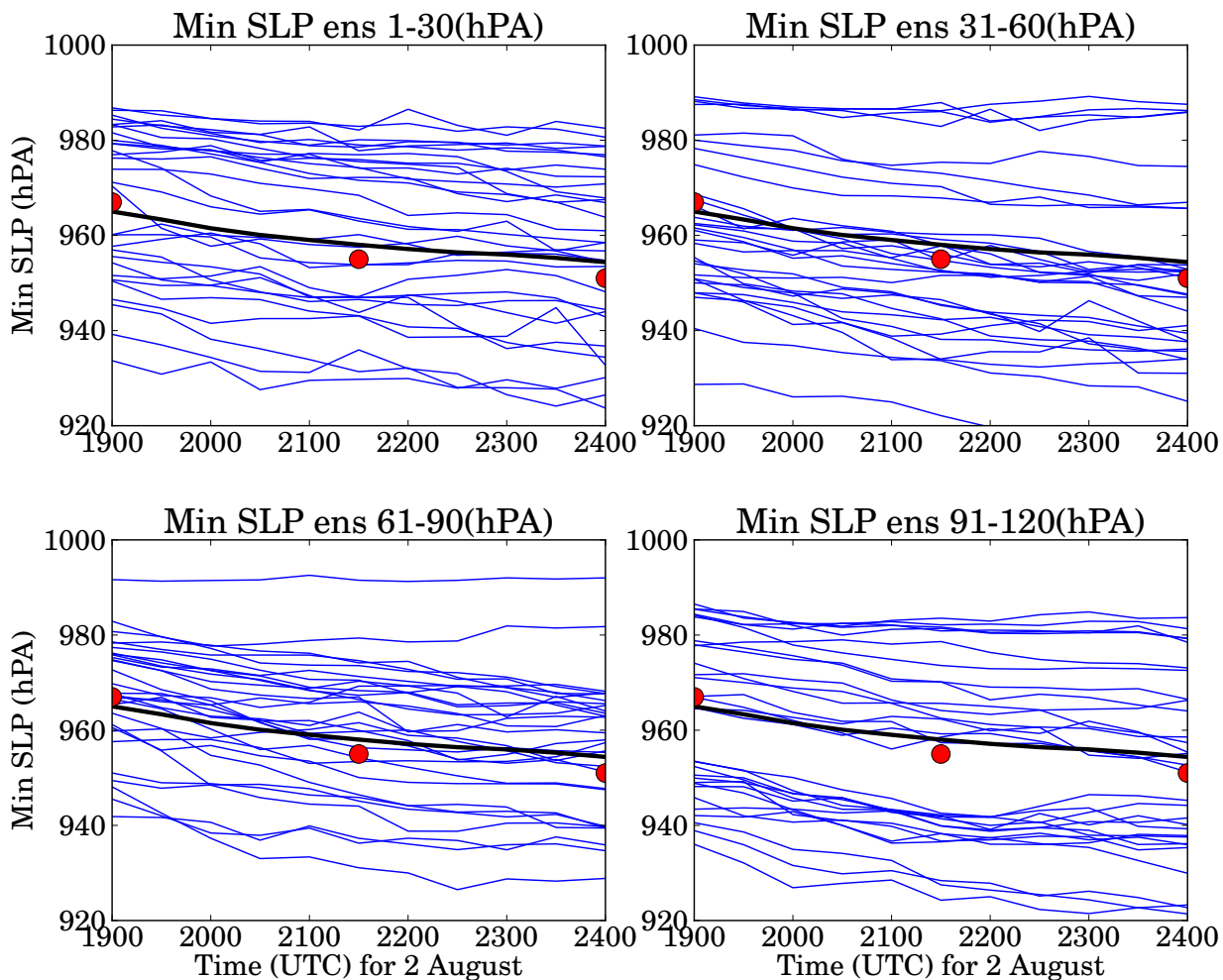


FIG. 4. Minimum sea level pressure versus simulation time for each ensemble member (blue line), ensemble average (black line), and observations (red dots), for ensemble 1-30 (top left), ensemble 31-60 (top right), ensemble 61-90 (bottom left), and ensemble 91-120 (bottom right).

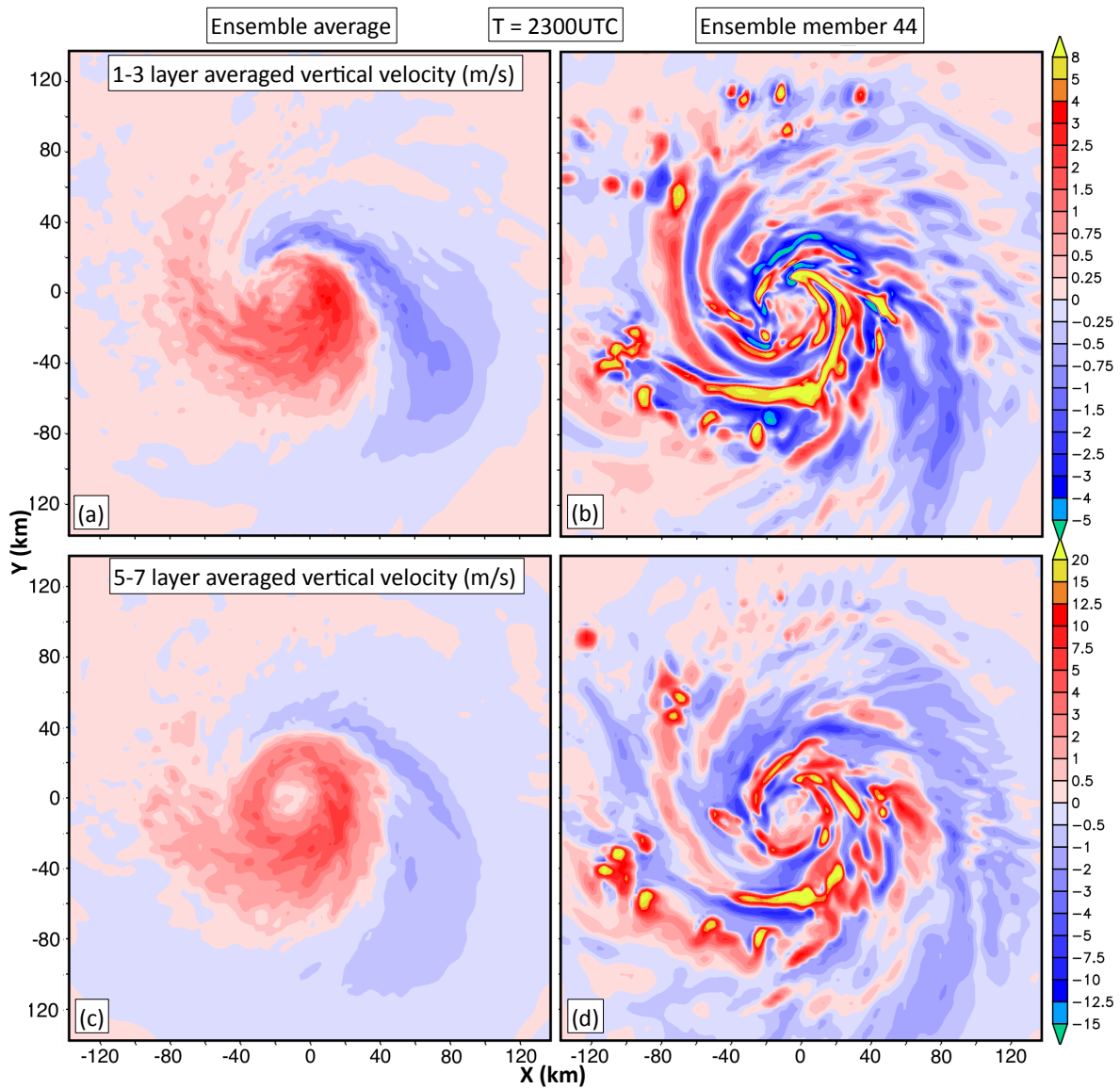


FIG. 5. Ensemble average vertical motion fields at 2300 UTC (11 hours into the simulations) averaged between 1-3 km (a) or 5-7 km (c). Corresponding layer-averaged vertical motions fields from ensemble member 44 between 1-3 km (b) or 5-7 km (d).

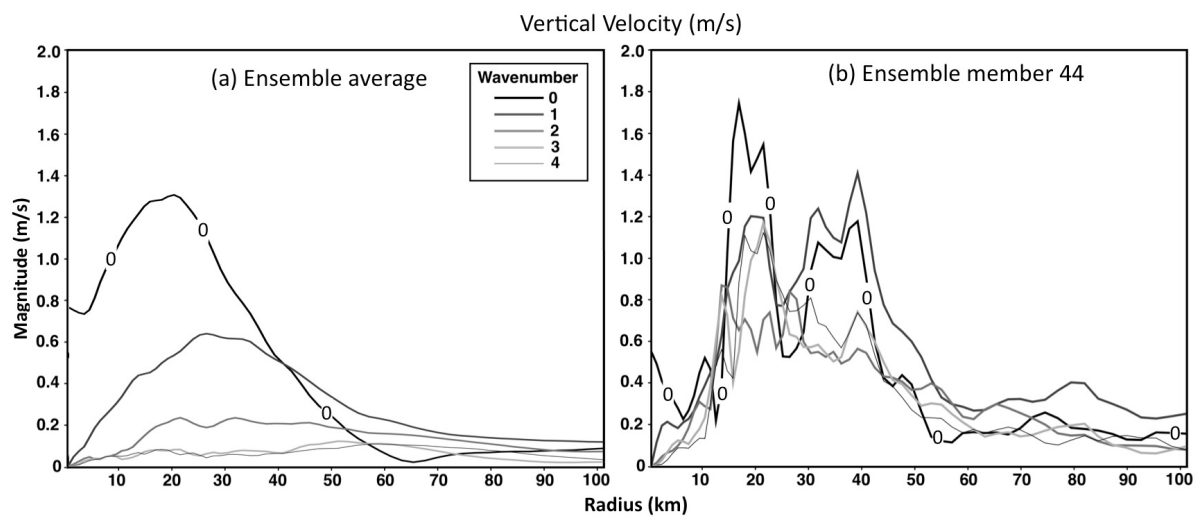


FIG. 6. Time-averaged axisymmetric (black solid line) and azimuthal wavenumber-14 amplitudes of vertical velocity in the 13-km layer within a 200 km radial distance from the storm center from the ensemble average (left figure) or ensemble 44 (right figure). The averaging times are between 2230 UTC and 2300 UTC.

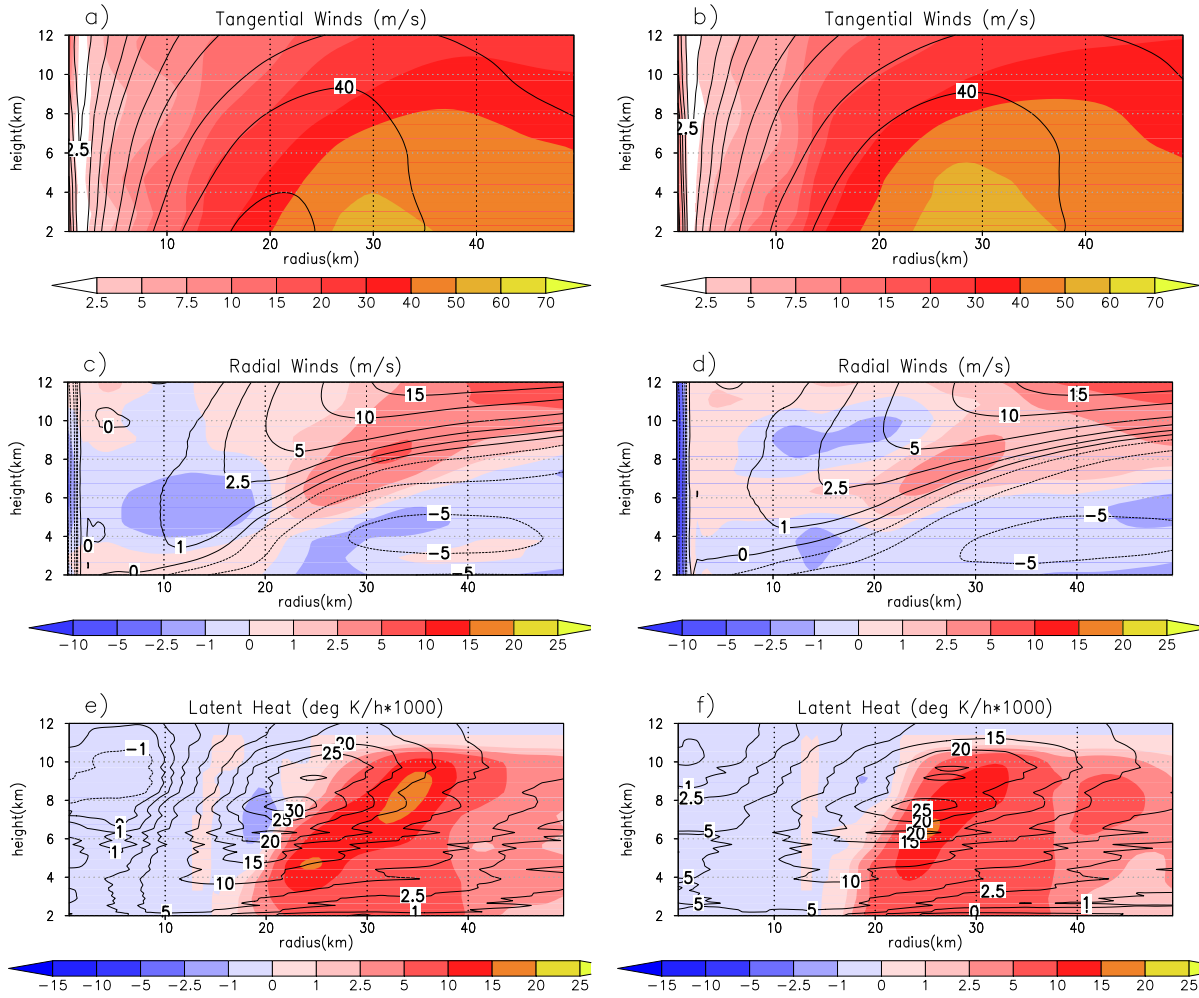


FIG. 7. Comparisons between azimuthally-averaged profiles for the ensemble average (contours) and observations (shaded) for tangential winds (top), radial winds (center), and latent heat (bottom). Time periods for comparisons are at flight leg 5 (2117 UTC) and 9 (2333 UTC).

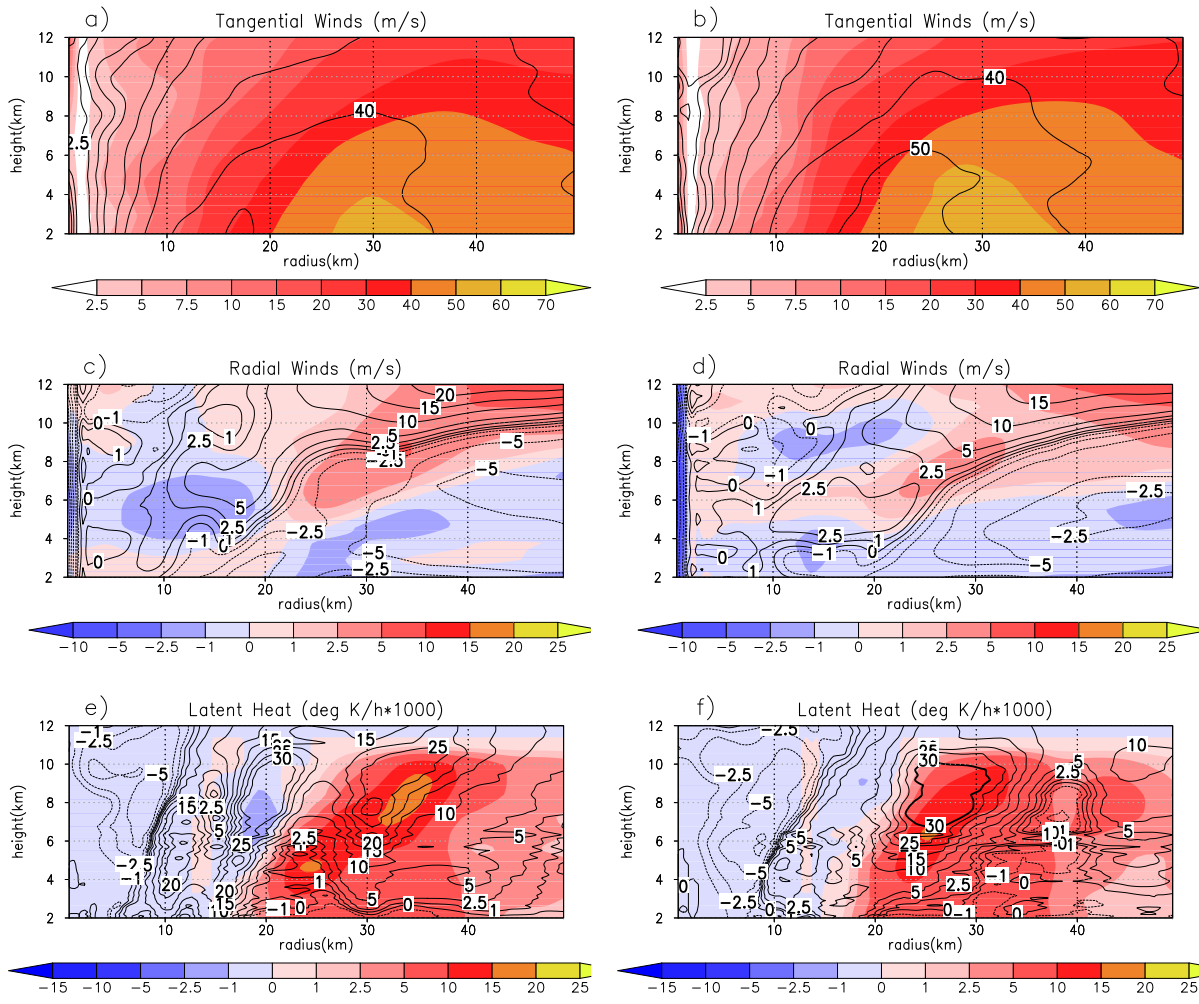


FIG. 8. Comparisons between azimuthally-averaged profiles for ensemble member 44 (contours) and observations (shaded) for tangential winds (top), radial winds (center), and latent heat (bottom). Time periods for comparisons are the same as in the previous figure.

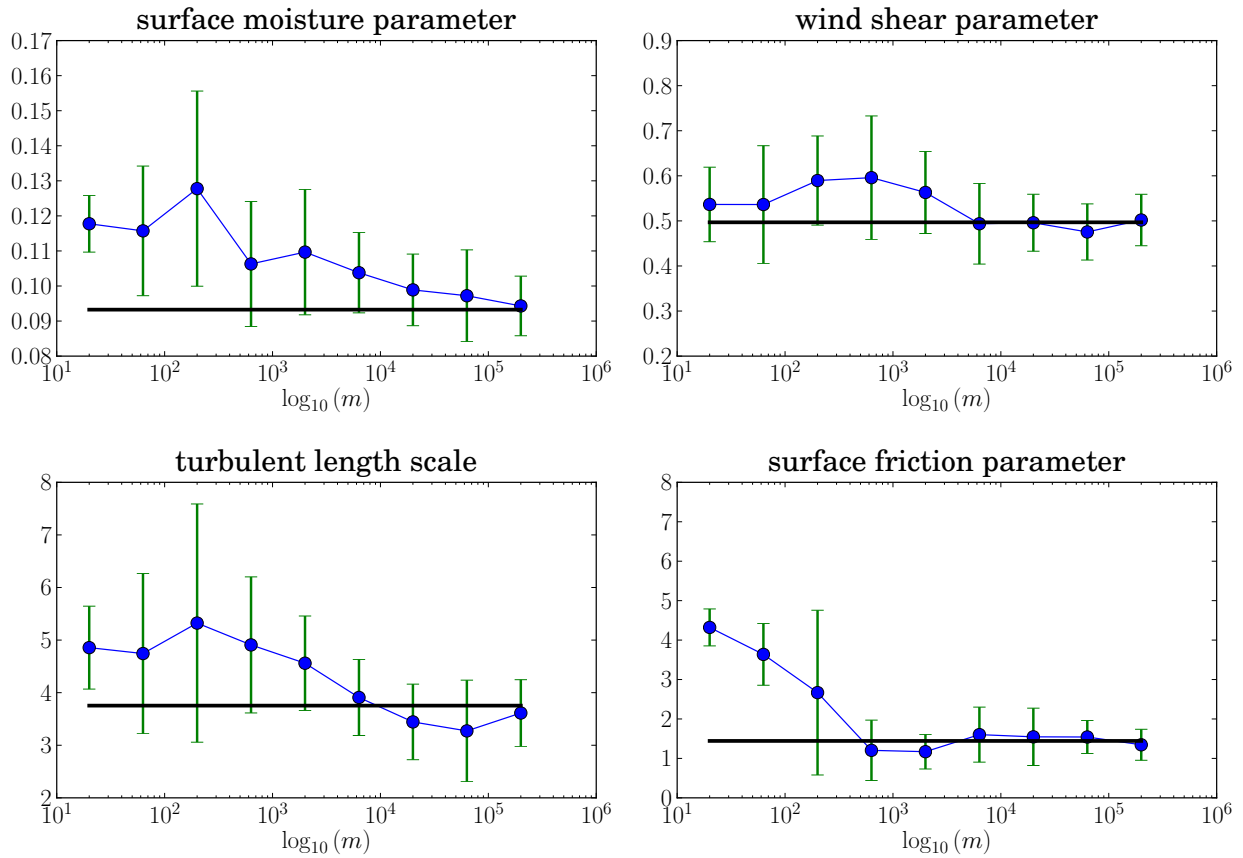


FIG. 9. EnKF parameter estimation as a function of number of latent heat observations assimilated. The latent heat observations were added in locations where the ensemble is most sensitive to changes in the parameters (Section 3.c).

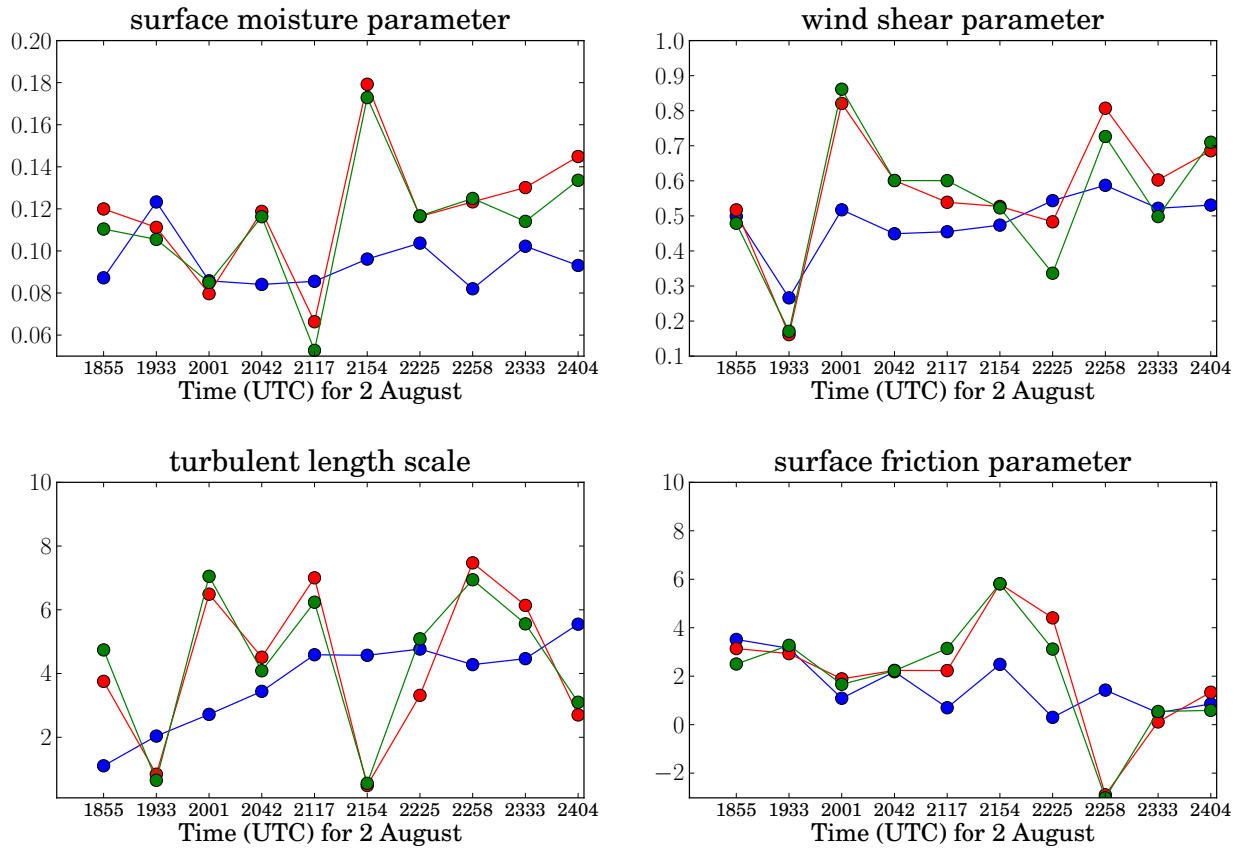


FIG. 10. Time distribution of the ensemble average parameter estimates with EnKF from DA1 (blue line, latent heat), DA2 (red line, horizontal winds), and DA3 (green line, both latent heat and horizontal winds).

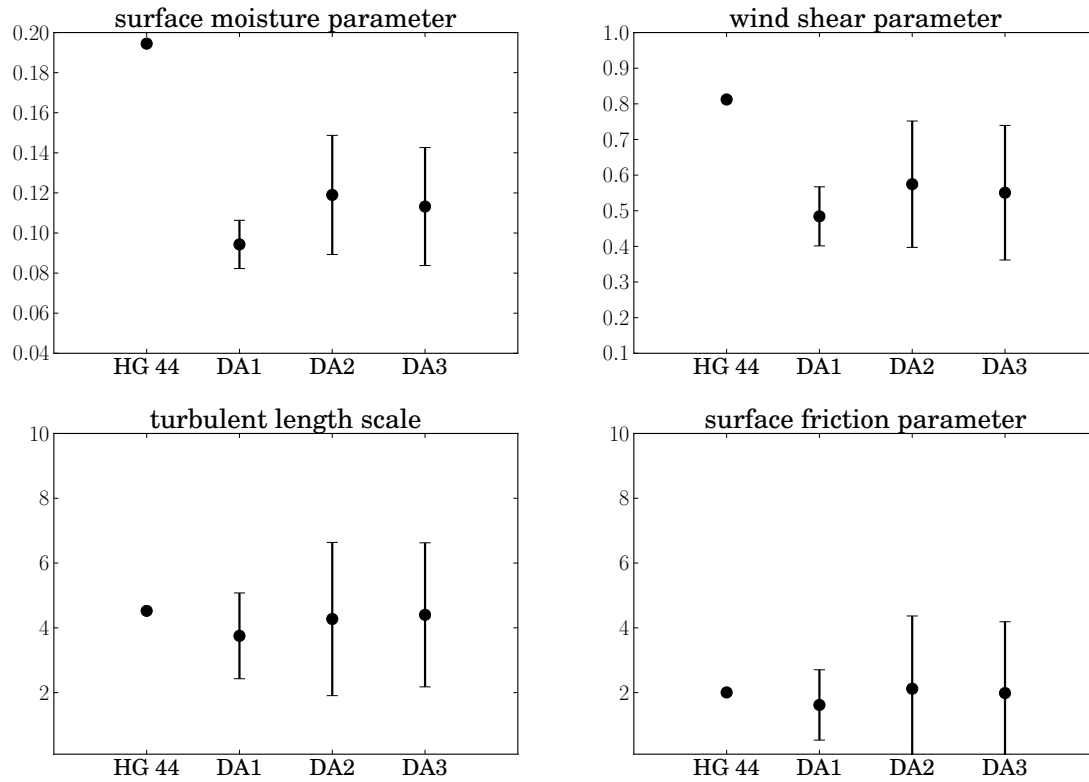


FIG. 11. Analysis parameters averaged over time for ensemble member 44 (HG 44), DA1, DA2, and DA3. The vertical lines from the dots indicate the time variance of the parameter estimates each experiment.

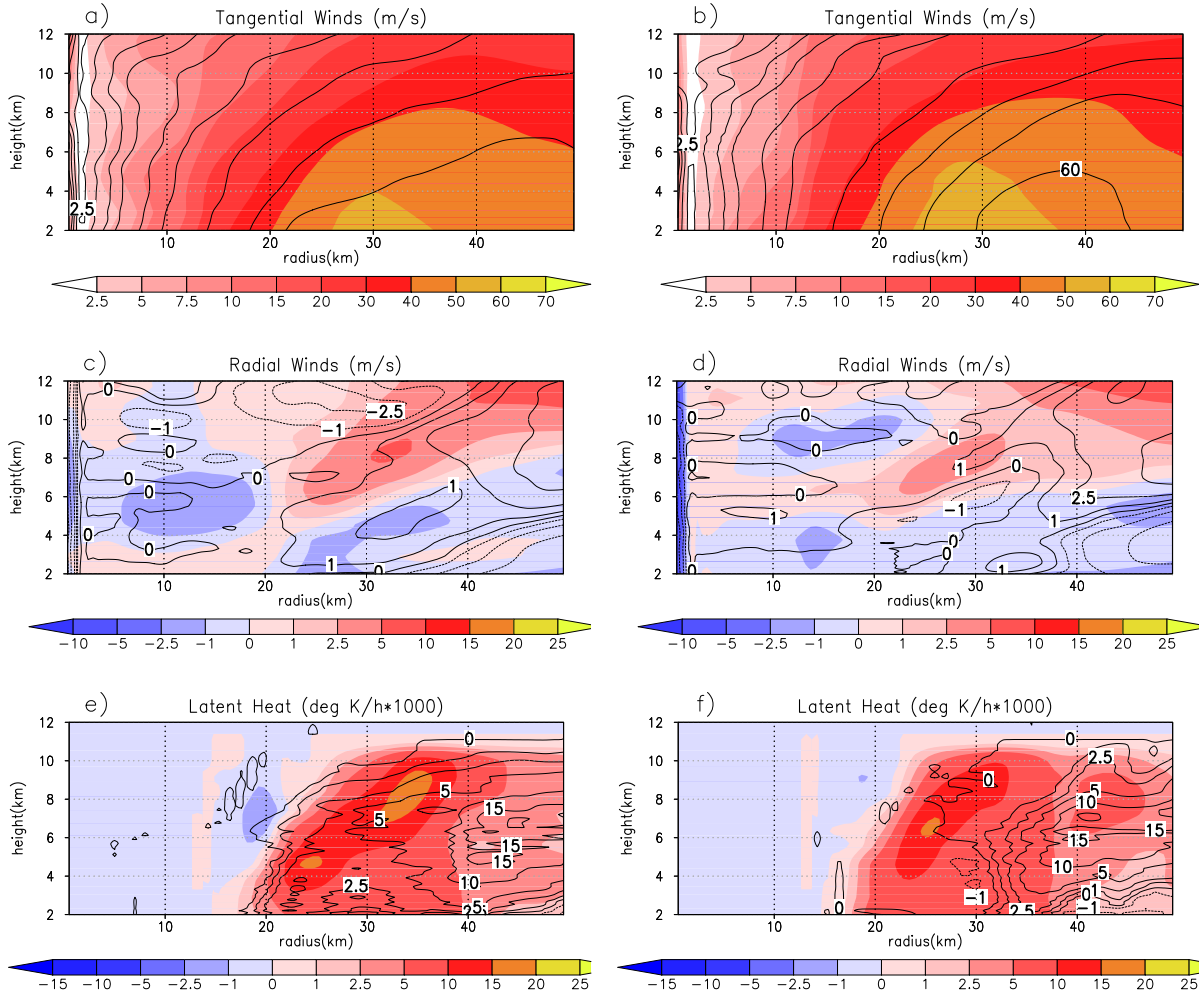


FIG. 12. Comparisons of the azimuthally-averaged profiles between a model simulation (contours) using estimated parameters from DA1 and observations (color shaded). Plots for tangential winds (top), radial winds (center), and latent heat (bottom) for flight leg 5 (2117 UTC) and 9 (2333 UTC).

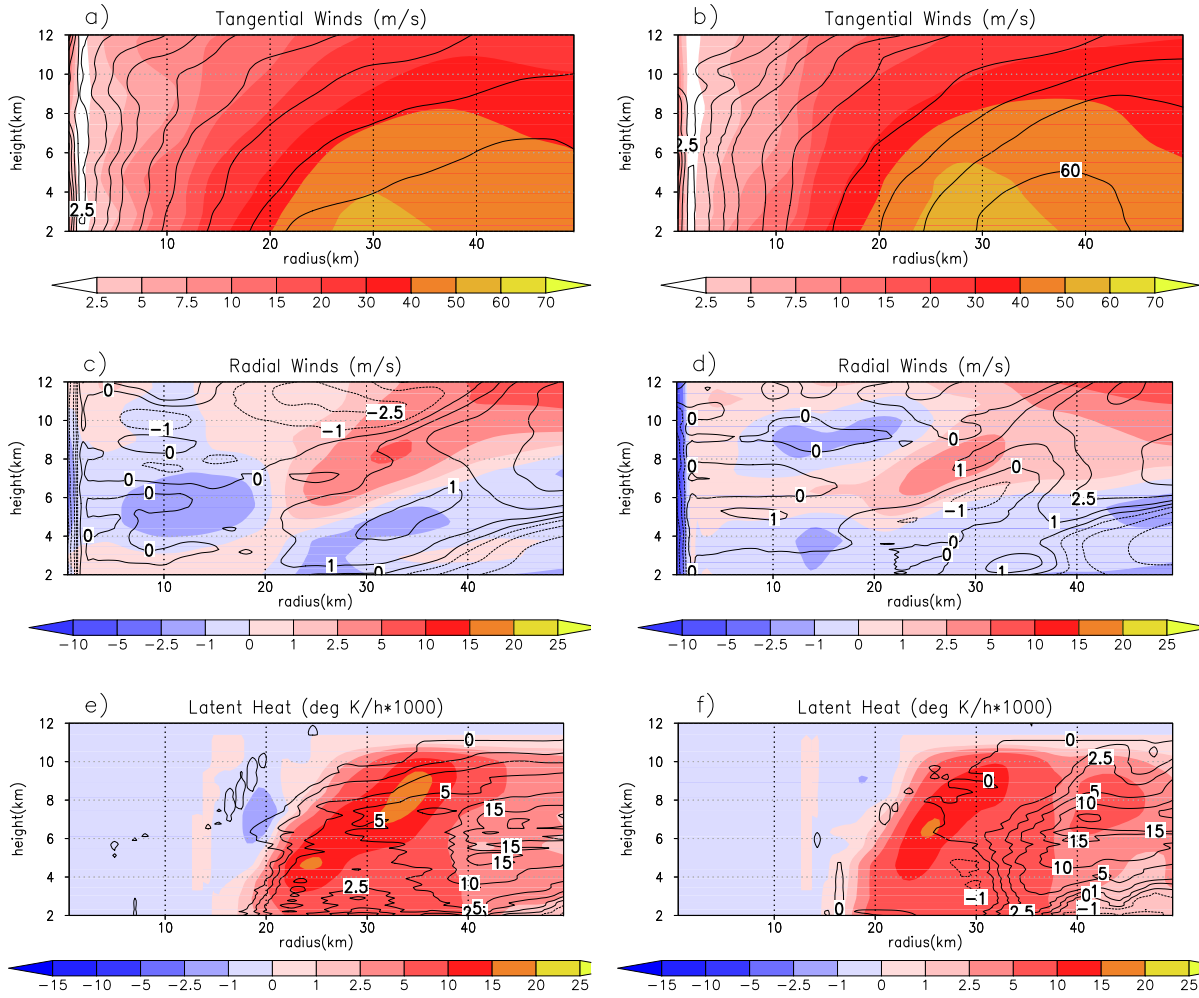


FIG. 13. Comparisons of the azimuthally-averaged profiles between a model simulation using estimated parameters from DA2 and observations (color shaded). Plots for tangential winds (top), radial winds (center), and latent heat (bottom) for the same time periods as in the previous figure.

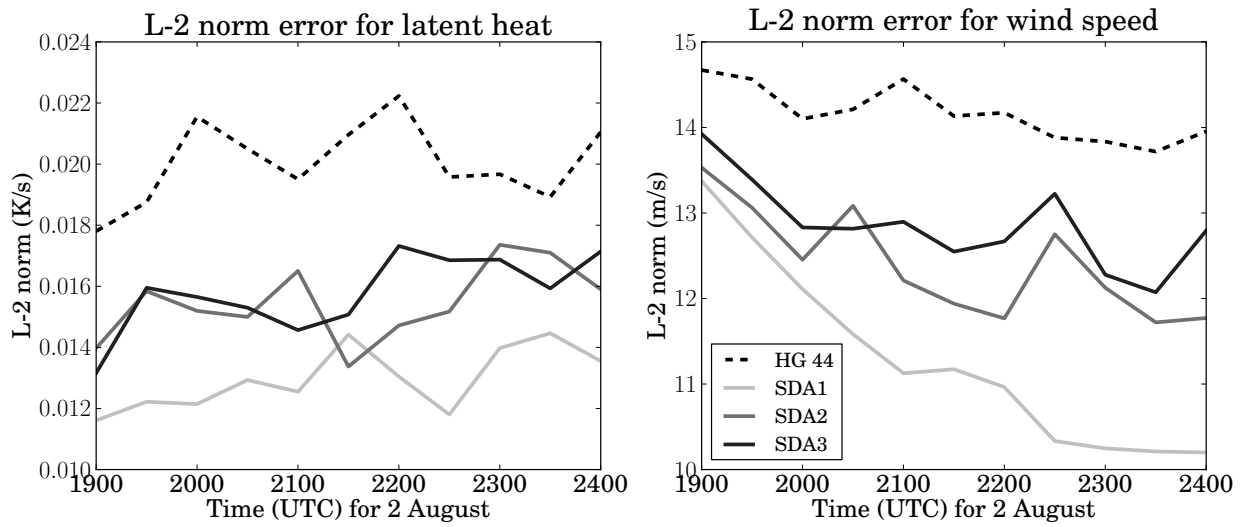


FIG. 14. Error estimates as a function of time computed using Eq. 20 of Reisner and Jeffery (2009) for ensemble member 44 (HG 44), SDA1, SDA2, and SDA3.

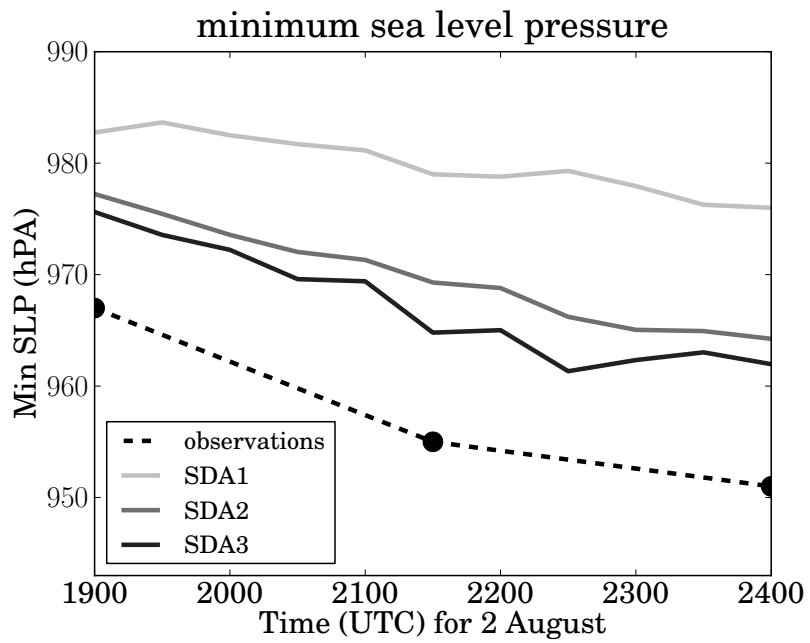


FIG. 15. Minimum sea level pressure for SDA1, SDA2, and SDA3 along with the observed pressure from Hurricane Guillermo.